
SELECTIVITY CONSIDERED HARMFUL: EVALUATING THE CAUSAL IMPACT OF CLASS SELECTIVITY IN DNNs

Matthew L. Leavitt,* Ari S. Morcos

Facebook AI Research

Menlo Park, CA, USA

{ito, arimorcos}@fb.com

ABSTRACT

The properties of individual neurons are often analyzed in order to understand the biological and artificial neural networks in which they’re embedded. Class selectivity—typically defined as how different a neuron’s responses are across different classes of stimuli or data samples—is commonly used for this purpose. However, it remains an open question whether it is necessary and/or sufficient for deep neural networks (DNNs) to learn class selectivity in individual units. We investigated the causal impact of class selectivity on network function by directly regularizing for or against class selectivity. Using this regularizer to reduce class selectivity across units in convolutional neural networks increased test accuracy by over 2% for ResNet18 trained on Tiny ImageNet. For ResNet20 trained on CIFAR10 we could reduce class selectivity by a factor of 2.5 with no impact on test accuracy, and reduce it nearly to zero with only a small ($\sim 2\%$) drop in test accuracy. In contrast, regularizing to increase class selectivity significantly decreased test accuracy across all models and datasets. These results indicate that class selectivity in individual units is neither sufficient nor strictly necessary, and can even impair DNN performance. They also encourage caution when focusing on the properties of single units as representative of the mechanisms by which DNNs function.

1 INTRODUCTION

Our ability to understand deep learning systems lags considerably behind our ability to obtain practical outcomes with them. A breadth of approaches have been developed in attempts to better understand deep learning systems and render them more comprehensible to humans (Yosinski et al., 2015; Bau et al., 2017; Olah et al., 2018; Hooker et al., 2019). Many of these approaches examine the properties of single neurons and treat them as representative of the networks in which they’re embedded (Erhan et al., 2009; Zeiler and Fergus, 2014; Karpathy et al., 2016; Amjad et al., 2018; Lillian et al., 2018; Dhamdhere et al., 2019; Olah et al., 2020).

The selectivity of individual units (i.e. the variability in a neuron’s responses across data classes or dimensions) is one property that has been of particular interest to researchers trying to better understand deep neural networks (DNNs) (Zhou et al., 2015; Olah et al., 2017; Morcos et al., 2018b; Zhou et al., 2018; Meyes et al., 2019; Na et al., 2019; Zhou et al., 2019; Rafegas et al., 2019; Bau et al., 2020). This focus on individual neurons makes intuitive sense, as the tractable, semantic nature of selectivity is extremely alluring; some measure of selectivity in individual units is often provided as an explanation of “what” a network is “doing”. One notable study highlighted a neuron selective for sentiment in an LSTM network trained on a word prediction task (Radford et al., 2017). Another attributed visualizable, semantic features to the activity of individual neurons across GoogLeNet trained on ImageNet (Olah et al., 2017). Both of these examples influenced many subsequent studies, demonstrating the widespread, intuitive appeal of “selectivity” (Amjad et al., 2018; Meyes et al., 2019; Morcos et al., 2018b; Zhou et al., 2015; 2018; Bau et al., 2017; Karpathy et al., 2016; Na et al., 2019; Radford et al., 2017; Rafegas et al., 2019; Morcos et al., 2018b; Olah et al., 2017; 2018; 2020).

Finding intuitive ways of representing the workings of DNNs is essential for making them understandable and accountable, but we must ensure that our approaches are based on meaningful properties of

*Work performed as part of the Facebook AI Residency

the system. Recent studies have begun to address this issue by investigating the relationships between selectivity and measures of network function such as generalization and robustness to perturbation (Morcos et al., 2018b; Zhou et al., 2018; Dalvi et al., 2019). Selectivity has also been used as the basis for targeted modulation of neural network function through individual units (Bau et al., 2019a;b).

However there is also growing evidence from experiments in both deep learning (Fong and Vedaldi, 2018; Morcos et al., 2018b; Gale et al., 2019; Donnelly and Roegiest, 2019) and neuroscience (Leavitt et al., 2017; Zylberberg, 2018; Insanally et al., 2019) that single unit selectivity may not be as important as once thought. Previous studies examining the functional role of selectivity in DNNs have often measured how selectivity mediates the effects of ablating single units, or used indirect, correlational approaches that modulate selectivity indirectly (e.g. batch norm) (Morcos et al., 2018b; Zhou et al., 2018; Lillian et al., 2018; Meyes et al., 2019; Kanda et al., 2020). But single unit ablation in trained networks has two critical limitations: it cannot address whether the *presence* of selectivity is beneficial, nor whether networks *need to learn* selectivity to function properly. It can only address the effect of removing a neuron from a network whose training process assumed the presence of that neuron. And even then, the observed effect might be misleading. For example, a property that is critical to network function may be replicated across multiple neurons. This redundancy means that ablating any one of these neurons would show little effect, and could thus lead to the erroneous conclusion that the examined property has little impact on network function.

We were motivated by these issues to pursue a series of experiments investigating the causal importance of class selectivity in artificial neural networks. To do so, we introduced a term to the loss function that allows us to directly regularize for or against class selectivity, giving us a single knob to control class selectivity in the network. The selectivity regularizer sidesteps the limitations of single unit ablation and other indirect techniques, allowing us to conduct a series of experiments evaluating the causal impact of class selectivity on DNN performance. Our findings are as follows:

- Performance can be improved by reducing class selectivity, suggesting that naturally-learned levels of class selectivity can be detrimental. Reducing class selectivity in ResNet18 trained on Tiny ImageNet could improve test accuracy by over 2%.
- Even when class selectivity isn’t detrimental to network function, it remains largely unnecessary. We reduced the mean class selectivity of units in ResNet20 trained on CIFAR10 by a factor of ~ 2.5 with no impact on test accuracy, and by a factor of ~ 20 —nearly to a mean of 0—with only a 2% change in test accuracy.
- Our regularizer does not simply cause networks to preserve class-selectivity by rotating it off of unit-aligned axes (i.e. by distributing selectivity linearly across units), but rather seems to suppress selectivity more generally, even when optimizing for high-selectivity basis sets. This demonstrates the viability of low-selectivity representations distributed *across* units.
- We show that regularizing to increase class selectivity, even by small amounts, has significant negative effects on performance. Trained networks seem to be perched precariously at a performance cliff with regard to class selectivity. These results indicate that the levels of class selectivity learned by individual units in the absence of explicit regularization are at the limit of what will impair the network.

Our findings collectively demonstrate that class selectivity in individual units is neither necessary nor sufficient for convolutional neural networks (CNNs) to perform image classification tasks, and in some cases can actually be detrimental. This alludes to the possibility of class selectivity regularization as a technique for improving CNN performance. More generally, our results encourage caution when focusing on the properties of single units as representative of the mechanisms by which CNNs function, and emphasize the importance of analyses that examine properties across neurons (i.e. distributed representations). Most importantly, our results are a reminder to verify that the properties we *do* focus on are actually relevant to CNN function.

2 RELATED WORK

2.1 SELECTIVITY IN DEEP LEARNING

Examining some form of selectivity in individual units constitutes the bedrock of many approaches to understanding DNNs. Sometimes the goal is simply to visualize selectivity, which has been pursued using a breadth of methods. These include identifying the input sample(s) (e.g. images) or sample

subregions that maximally activate a given neuron (Zhou et al., 2015; Rafegas et al., 2019), and numerous optimization-based techniques for generating samples that maximize unit activations (Erhan et al., 2009; Zeiler and Fergus, 2014; Simonyan et al., 2014; Yosinski et al., 2015; Nguyen et al., 2016; Olah et al., 2017; 2018). While the different methods for quantifying single unit selectivity are often conceptually quite similar (measuring how variable are a neuron's responses across different classes of data samples), they have been applied across a broad range of contexts (Amjad et al., 2018; Meyes et al., 2019; Morcos et al., 2018b; Zhou et al., 2015; 2018; Bau et al., 2017; Karpathy et al., 2016; Na et al., 2019; Radford et al., 2017; Rafegas et al., 2019). For example, Bau et al. (2017) quantified single unit selectivity for "concepts" (as annotated by humans) in networks trained for object and scene recognition. Olah et al. (2018; 2020) have pursued a research program examining single unit selectivity as a building block for understanding DNNs. And single units in models trained to solve natural language processing tasks have been found to exhibit selectivity for syntactical and semantic features (Karpathy et al., 2016; Na et al., 2019), of which the "sentiment-selective neuron" reported by Radford et al. (2017) is a particularly recognized example.

The relationship between individual unit selectivity and various measures of DNN performance have been examined in prior studies, but the conclusions have not been concordant. Morcos et al. (2018b), using single unit ablation and other techniques, found that a network's test set generalization is negatively correlated (or uncorrelated) with the class selectivity of its units, a finding replicated by Kanda et al. (2020). In contrast, though Amjad et al. (2018) confirmed these results for single unit ablation, they also performed cumulative ablation analyses which suggested that selectivity is beneficial, suggesting that redundancy across units may make it difficult to interpret single unit ablation studies.

In a follow-up study, Zhou et al. (2018) found that ablating class-selective units impairs classification accuracy for specific classes (though interestingly, not always the same class the unit was selective for), but a compensatory increase in accuracy for other classes can often leave overall accuracy unaffected. Ukita (2018) found that orientation selectivity in individual units is correlated with generalization performance in convolutional neural networks (CNNs), and that ablating highly orientation-selective units impairs classification accuracy more than ablating units with low orientation-selectivity. But while orientation selectivity and class selectivity can both be considered types of feature selectivity, orientation selectivity is far less abstract and focuses on specific properties of the image (e.g., oriented edges) rather than semantically meaningful concepts and classes. Nevertheless, this study still demonstrates the importance of some types of selectivity.

Results are also variable for models trained on NLP tasks. Dalvi et al. (2019) found that ablating units selective for linguistic features causes greater performance deficits than ablating less-selective units, while Donnelly and Roegiest (2019) found that ablating the "sentiment neuron" of Radford et al. (2017) has equivocal effects on performance. These findings seem challenging to reconcile.

All of these studies examining class selectivity in single units are hamstrung by their reliance on single unit ablation, which could account for their conflicting results. As discussed earlier, single unit ablation can only address whether class selectivity affects performance in trained networks, and not whether individual units to *need to learn* class selectivity for optimal network function. And even then, the conclusions obtained from single neuron ablation analyses can be misleading due to redundancy across units (Amjad et al., 2018; Meyes et al., 2019).

2.2 SELECTIVITY IN NEUROSCIENCE

Measuring the responses of single neurons to a relevant set of stimuli has been the canonical first-order approach for understanding the nervous system (Sherrington, 1906; Adrian, 1926; Granit, 1955; Hubel and Wiesel, 1959; Barlow, 1972; Kandel et al., 2000); its application has yielded multiple Nobel Prizes (Hubel and Wiesel, 1959; 1962; Hubel, 1982; Wiesel, 1982; O'Keefe and Dostrovsky, 1971; Fyhn et al., 2004). But recent experimental findings have raised doubts about the necessity of selectivity for high-fidelity representations in neuronal populations (Leavitt et al., 2017; Insanally et al., 2019; Zylberberg, 2018), and neuroscience research seems to be moving beyond characterizing neural systems at the level of single neurons, towards population-level phenomena (Shenoy et al., 2013; Raposo et al., 2014; Fusi et al., 2016; Morcos and Harvey, 2016; Pruszynski and Zylberberg, 2019; Heeger and Mackey, 2019; Saxena and Cunningham, 2019).

Single unit selectivity-based approaches are ubiquitous in attempts to understand artificial and biological neural systems, but growing evidence has led to questions about the importance of focusing on selectivity and its role in DNN function. These factors, combined with the limitations of prior approaches, lead to the question: is class selectivity necessary and/or sufficient for DNN function?

3 APPROACH

Networks naturally seem to learn solutions that result in class-selective individual units (Zhou et al., 2015; Olah et al., 2017; Morcos et al., 2018b; Zhou et al., 2018; Meyes et al., 2019; Na et al., 2019; Zhou et al., 2019; Rafegas et al., 2019; Amjad et al., 2018; Meyes et al., 2019; Bau et al., 2017; Karpathy et al., 2016; Radford et al., 2017; Olah et al., 2018; 2020). We examined whether learning class-selective representations in individual units is actually necessary for networks to function properly. Motivated by the limitations of single unit ablation techniques and the indirectness of using batch norm or dropout to modulate class selectivity (e.g. Morcos et al. (2018b); Zhou et al. (2018); Lillian et al. (2018); Meyes et al. (2019)), we developed an alternative approach for examining the necessity of class selectivity for network performance. By adding a term to the loss function that serves as a regularizer to suppress (or increase) class selectivity, we demonstrate that it is possible to directly modulate the amount of class selectivity in all units in aggregate. We then used this approach as the basis for a series of experiments in which we modulated levels of class selectivity across individual units and measured the resulting effects on the network. Critically, the selectivity regularizer sidesteps the limitations of single unit ablation-based approaches, allowing us to answer otherwise-inaccessible questions such as whether single units actually need to learn class selectivity, and whether increased levels of class selectivity are beneficial.

Unless otherwise noted: all experimental results were derived from the test set with the parameters from the epoch that achieved the highest validation set accuracy over the training epochs; 20 replicates with different random seeds were run for each hyperparameter set; error bars and shaded regions denote bootstrapped 95% confidence intervals; selectivity regularization was not applied to the final (output) layer, nor was the final layer included in any of our analyses because by definition the output layer must be class selective in a classification task.

3.1 MODELS AND DATASETS

Our experiments were performed on ResNet18 (He et al., 2016) trained on Tiny ImageNet (Fei-Fei et al., 2015), and ResNet20 (He et al., 2016) and a VGG16-like network (Simonyan and Zisserman, 2015), both trained on CIFAR10 (Krizhevsky, 2009). Additional details about hyperparameters, data, training, and software are in Appendix A.1. We focus on Tiny ImageNet in the main text, but results were qualitatively similar across models and datasets except where noted.

3.2 DEFINING CLASS SELECTIVITY

There are a breadth of approaches for quantifying class selectivity in individual units (Moody et al., 1998; Zhou et al., 2015; Li et al., 2015; Zhou et al., 2018; Gale et al., 2019). We chose the neuroscience-inspired approach of Morcos et al. (2018b) because it is similar to many widely-used metrics, easy to compute, and most importantly, differentiable (the utility of this is addressed in the next section). We also confirmed the efficacy of our regularizer on a different, non-differentiable selectivity metric (see Appendix A.13). For a single convolutional feature map (which we refer to as a "unit"), we computed the mean activation across elements of the filter map in response to a single sample, after the non-linearity. Then the class-conditional mean activation (i.e. the mean activation for each class) was calculated across all samples in the test set, and the class selectivity index (SI) was calculated as follows:

$$SI = \frac{\mu_{max} - \mu_{-max}}{\mu_{max} + \mu_{-max} + \epsilon} \quad (1)$$

where μ_{max} is the largest class-conditional mean activation, μ_{-max} is the mean response to the remaining (i.e. non- μ_{max}) classes, and ϵ is a small value to prevent division by zero (we used 10^{-7}) in the case of a dead unit. The selectivity index can range from 0 to 1. A unit with identical average activity for all classes would have a selectivity of 0, and a unit that only responded to a single class would have a selectivity of 1.

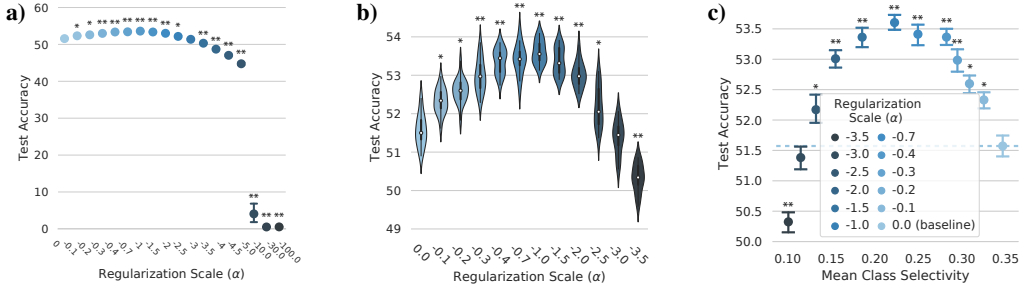


Figure 1: Effects of reducing class selectivity on test accuracy in ResNet18 trained on Tiny Imagenet. (a) Test accuracy (y-axis) as a function of regularization scale (α , x-axis and intensity of blue). **(b)** Identical to **(a)**, but for a subset of α values. The center of each violin plot contains a boxplot, in which the darker central lines denote the central two quartiles. **(c)** Test accuracy (y-axis) as a function of mean class selectivity (x-axis) for different values of α . Error bars denote 95% confidence intervals. $*p < 0.01$, $**p < 5 \times 10^{-10}$ difference from $\alpha = 0$, t-test, Bonferroni-corrected. See Appendix A.4 and A.12 for ResNet20 and VGG results, respectively.

As Morcos et al. (2018b) note, this selectivity index is not a perfect measure of information content in single units. For example, a unit with some information about many classes would have a low selectivity index. But it achieves the goal of identifying units that are class-selective in a similarly intuitive way as prior studies (Zhou et al., 2018), while also being differentiable with respect to the model parameters.

3.3 A SINGLE KNOB TO CONTROL CLASS SELECTIVITY

Because the class selectivity index is differentiable, we can insert it into the loss function, allowing us to directly regularize for or against class selectivity. Our loss function, which we seek to minimize, thus takes the following form:

$$\text{loss} = - \sum_c^C y_c \cdot \log(\hat{y}_c) - \alpha \mu_{SI} \quad (2)$$

The left-hand term in the loss function is the traditional cross-entropy between the softmax of the output units and the true class labels, where c is the class index, C is the number of classes, y_c is the true class label, and \hat{y}_c is the predicted class probability. We refer to the right-hand component of the loss function, $-\alpha \mu_{SI}$, as the class selectivity regularizer (or regularizer, for brevity). The regularizer consists of two terms: the selectivity term,

$$\mu_{SI} = \frac{1}{L} \sum_l^L \frac{1}{U} \sum_u^U SI_u \quad (3)$$

where l is a convolutional layer, L is number of layers, u is a unit (i.e. feature map), U is the number of units in a given layer, and SI_u is the class selectivity index of unit u . The selectivity term of the regularizer is obtained by computing the selectivity index for each unit in a layer, then computing the mean selectivity index across units within each layer, then computing the mean selectivity index across layers. Computing the mean within layers before computing the mean across layers (as compared to computing the mean across all units in the network) mitigates the biases induced by the larger numbers of units in deeper layers. The remaining term in the regularizer is α , the regularizer scale. The sign of α determines whether class selectivity is promoted or discouraged. Negative values of α discourage class selectivity in individual units, while positive values promote it. The magnitude of α controls the contribution of the selectivity term to the overall loss. α thus serves as a single knob with which we can modulate class selectivity across all units in the network in aggregate. During training, the class selectivity index was computed for each minibatch. For the results presented here, the class selectivity index was computed across the entire test set. We also experimented with restricting regularization to the first or final three layers, which yielded qualitatively similar results (Appendix A.14).

4 RESULTS

4.1 TEST ACCURACY IS IMPROVED OR UNAFFECTED BY REDUCING CLASS SELECTIVITY

Prior research has yielded equivocal results regarding the importance of class selectivity in individual units. We sidestepped the limitations of previous approaches by regularizing against selectivity directly in the loss function through the addition of the selectivity term (see Approach 3.3), giving us a knob with which to causally manipulate class selectivity. We first verified that the regularizer works

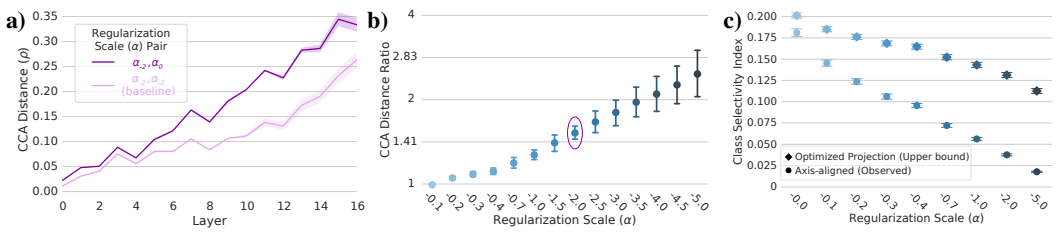


Figure 2: Checking for off-axis selectivity. (a) Mean CCA distance (ρ , y-axis) as a function of layer (x-axis) between pairs of replicate ResNet18 networks (see Section 4.2 or Appendix A.3.2) trained with $\alpha = -2$ (i.e. $\rho(\alpha_{-2}, \alpha_{-2})$; light purple), and between pairs of networks trained with $\alpha = -2$ and $\alpha = 0$ (i.e. $\rho(\alpha_{-2}, \alpha_0)$; dark purple). (b) For each layer, we compute the ratio of $\rho(\alpha_{-2}, \alpha_0) : \rho(\alpha_{-1}, \alpha_{-2})$, which we refer to as the CCA distance ratio. We then plot the mean CCA distance ratio across layers (y-axis) as a function of α (x-axis, intensity of blue). Example from panel a ($\alpha = -2$) circled in purple. $p < 1.3 \times 10^{-5}$, paired t-test, for all α except -0.1. (c) Mean class selectivity (y-axis) as a function of regularization scale (α ; x-axis) for ResNet18 trained on Tiny ImageNet. Diamond-shaped data points denote the upper bound on class selectivity for a linear projection of activations (see Section 4.2 or Appendix A.7), while circular points denote the amount of axis-aligned class selectivity for the corresponding values of α . Error bars or shaded region = 95% confidence intervals. ResNet20 results are in Appendix A.6 (CCA) and A.7 (selectivity upper bound).

as intended (Figure A1). Indeed, class selectivity across units in a network decreases as α becomes more negative. We also confirmed that our class selectivity regularizer has a similar effect when measured using a different class selectivity metric (see Appendix A.13), indicating that our results are not unique to the metric used in our regularizer. The regularizer thus allows us to examine the causal impact of class selectivity on test accuracy.

Regularizing against class selectivity could yield three possible outcomes: If the previously-reported anti-correlation between selectivity and generalization is causal, then test accuracy should increase. But if class selectivity is necessary for high-fidelity class representations, then we should observe a decrease in test accuracy. Finally, if class selectivity is an emergent phenomenon and/or irrelevant to network performance, test accuracy should remain unchanged.

Surprisingly, we observed that reducing selectivity significantly improves test accuracy in ResNet18 trained on Tiny ImageNet for all examined values of $\alpha \in [-0.1, -2.5]$ (Figure 1; $p < 0.01$, Bonferroni-corrected t-test). Test accuracy increases with the magnitude of α , reaching a maximum at $\alpha = -1.0$ (test accuracy at $\alpha_{-1.0} = 53.60 \pm 0.13$, α_0 (i.e. no regularization) = 51.57 ± 0.18), at which point there is a 1.6x reduction in class selectivity (mean class selectivity at $\alpha_{-1.0} = 0.22 \pm 0.0009$, $\alpha_0 = 0.35 \pm 0.0007$). Test accuracy then begins to decline; at $\alpha_{-3.0}$ test accuracy is statistically indistinct from α_0 , despite a 3x decrease in class selectivity (mean class selectivity at $\alpha_{-3.0} = 0.12 \pm 0.0007$, $\alpha_0 = 0.35 \pm 0.0007$). Further reducing class selectivity beyond $\alpha = -3.5$ (mean class selectivity = 0.10 ± 0.0007) has increasingly detrimental effects on test accuracy. These results show that the amount of class selectivity naturally learned by a network (i.e. the amount learned in the absence of explicit regularization) can actually constrain the network’s performance.

ResNet20 trained on CIFAR10 also learned superfluous class selectivity. Although reducing class selectivity does not improve performance, it causes minimal detriment, except at extreme regularization scales ($\alpha \leq -30$; Figure A2). Increasing the magnitude of α decreases mean class selectivity across the network, with little impact on test accuracy until mean class selectivity reaches 0.003 ± 0.0002 at α_{-30} (Figure A1d). Reducing class selectivity only begins to have a statistically significant effect on performance at $\alpha_{-1.0}$ (Figure A2a), at which point mean class selectivity across the network has decreased from 0.22 ± 0.002 at α_0 (i.e. no regularization) to 0.07 ± 0.0013 at $\alpha_{-1.0}$ —a factor of more than 3 (Figure A2c; $p = 0.03$, Bonferroni-corrected t-test). This implies that ResNet20 learns more than three times the amount of class selectivity required for maximum test accuracy.

We observed qualitatively similar results for VGG16 (see Appendix A.12). Although the difference is significant at $\alpha = -0.1$ ($p = 0.004$, Bonferroni-corrected t-test), it is possible to reduce mean class selectivity by a factor of 5 with only a 0.5% decrease in test accuracy, and by a factor of 10 with only a ~1% drop in test accuracy. These differences may be due to VGG16’s naturally higher levels of class selectivity (see Appendix A.15 for comparisons between VGG16 and ResNet20). Together, these results demonstrate that class selectivity in individual units is largely unnecessary for optimal performance in CNNs trained on image classification tasks.

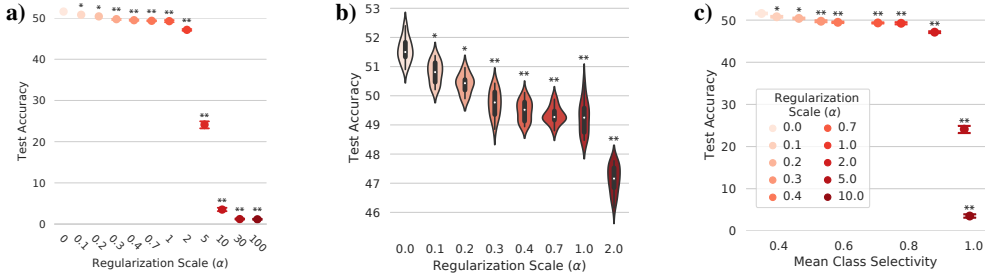


Figure 3: Effects of increasing class selectivity on test accuracy in ResNet18 trained on Tiny ImageNet.

(a) Test accuracy (y-axis) as a function of regularization scale (α ; x-axis, intensity of red). (b) Identical to (a), but for a subset of α values. Each violin plot contains a boxplot in which the darker central lines denote the central two quartiles. (c) Test accuracy (y-axis) as a function of mean class selectivity (x-axis) across α values. Error bars denote 95% confidence intervals. $*p < 6 \times 10^{-5}$, $**p < 8 \times 10^{-12}$ difference from $\alpha = 0$, t-test, Bonferroni-corrected. See Appendix A.9 and A.12 for ResNet20 and VGG results, respectively.

4.2 DOES SELECTIVITY SHIFT TO A DIFFERENT BASIS SET?

We were able to reduce mean class selectivity in all examined networks by a factor of at least three with minimal negative impact on test accuracy ($\sim 1\%$, at worst, for VGG16). However, one trivial solution for reducing class selectivity is for the network to "hide" it from the regularizer by rotating it off of unit-aligned axes or performing some other linear transformation. In this scenario the selectivity in individual units would be reduced, but remain accessible through linear combinations of activity across units. In order to test this possibility, we used CCA (see Appendix A.3), which is invariant to rotation and other invertible affine transformations, to compare the representations in regularized (i.e. low-selectivity) networks to the representations in unregularized networks.

We first established a meaningful baseline for comparison by computing the CCA distances between each pair of 20 replicate networks for a given value of α (we refer to this set of distances as $\rho(\alpha_r, \alpha_r)$). If regularizing against class selectivity causes the network to move selectivity off-axis, the CCA distances between regularized and unregularized networks—which we term $\rho(\alpha_r, \alpha_0)$ —should be similar to $\rho(\alpha_r, \alpha_r)$. Alternatively, if class selectivity is suppressed via some non-affine transformation of the representation, $\rho(\alpha_r, \alpha_0)$ should exceed $\rho(\alpha_r, \alpha_r)$.

Our analyses confirm the latter hypothesis: we find that $\rho(\alpha_r, \alpha_0)$ significantly exceeds $\rho(\alpha_r, \alpha_r)$ for all values of α except $\alpha = -0.1$ in ResNet18 trained on Tiny ImageNet (Figure 2 $p < 1.3 \times 10^{-5}$, paired t-test). The effect is even more striking in ResNet20 trained on CIFAR10; all tested values of α are significant (Figure A3; $p < 5 \times 10^6$, paired t-test). Furthermore, the size of the effect is proportional to α in both models; larger α values yield representations that are more dissimilar to unregularized representations. These results support the conclusion that our regularizer doesn't just cause class selectivity to be rotated off of unit-aligned axes, but also suppresses it.

As an additional control to ensure that our regularizer did not simply shift class selectivity to off-axis directions in activation space, we calculated an upper bound on the amount of class selectivity that could be recovered by finding the linear projection of unit activations that maximizes class selectivity (see Appendix A.7 for methodological details). For both ResNet18 trained on Tiny ImageNet (Figure 2c) and ResNet20 trained on CIFAR10 (Figure A4b), the amount of class selectivity in the optimized projection decreases as a function of increasing $|\alpha|$, indicating that regularizing against class selectivity does not simply rotate the selectivity off-axis. Interestingly, the upper bound on class selectivity is very similar across regularization scales in the final two convolutional layers in both models (Figure A4a; A4c), indicating that immediate proximity to the output layer may mitigate the effect of class selectivity regularization. While we also found that the amount of class selectivity in the optimized projection is consistently higher than the observed axis-aligned class selectivity, we consider this to be an expected result, as the optimized projection represents an upper bound on the amount class selectivity that could be recovered from the models' representations. However, the decreasing upper bound as a function of increasing $|\alpha|$ indicates that our class selectivity regularizer decreases selectivity across all basis sets, and not just along unit-aligned axes.

4.3 INCREASED CLASS SELECTIVITY CONSIDERED HARMFUL

We have demonstrated that class selectivity can be significantly reduced with minimal impact on test accuracy. However, we only examined the effects of *reducing* selectivity. What are the effects of *increasing* selectivity? We examined this question by regularizing *for* class selectivity, instead of against it. This is achieved quite easily, as it requires only a change in the sign of α . We first

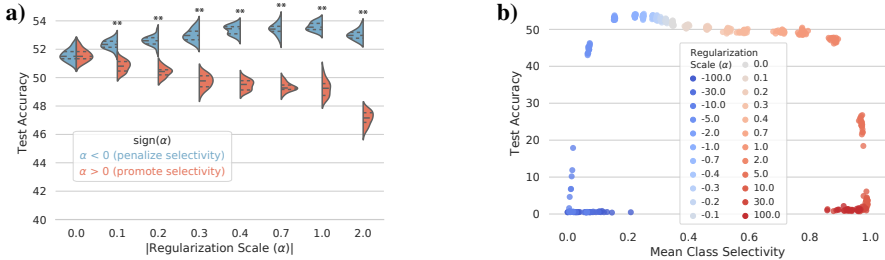


Figure 4: Increasing class selectivity has deleterious effects on test accuracy compared to reducing class selectivity. (a) Test accuracy (y-axis) as a function of regularization scale magnitude ($|\alpha|$) for negative (blue) vs positive (red) values of α . Solid line in distributions denotes mean, dashed line denotes central two quartiles. $**p < 6 \times 10^{-6}$ difference between $\alpha < 0$ and $\alpha > 0$, Wilcoxon rank-sum test, Bonferroni-corrected. (b) Test accuracy (y-axis) as a function of mean class selectivity (x-axis). All results shown are for ResNet18.

confirmed that changing the sign of the scale term in the loss function causes the intended effect of increasing class selectivity in individual units (see Appendix A.8).

Despite class selectivity not being strictly necessary for high performance, its ubiquity across biological and artificial neural networks leads us to suspect it may still be sufficient. We thus expect that increasing it would either improve test accuracy or yield no effect. For the same reason, we would consider it unexpected if increasing selectivity impairs test accuracy.

Surprisingly, we observe the latter outcome: increasing class selectivity negatively impacts network performance in ResNet18 trained on Tiny ImageNet (Figure 3a). Scaling the regularization has an immediate effect: a significant decline in test accuracy is present even at the smallest tested value of α ($p \leq 6 \times 10^{-5}$ for all α , Bonferroni-corrected t-test) and falls catastrophically to $\sim 25\%$ by $\alpha = 5.0$. The effect proceeds even more dramatically in ResNet20 trained on CIFAR10 (Figure A6a). Note that we observed a correlation between the strength of regularization and the presence of dead units in ResNet20, but further analyses ruled this out as an explanation for the decline in test accuracy (see Appendix A.10). One solution to generate a very high selectivity index is if a unit is silent for the vast majority of inputs and has low activations for remaining set of inputs. If this were the case, we would expect that regularizing to increase selectivity would cause units to be silent for the majority of inputs. However, we found that the majority of units were active for $\geq 80\%$ of inputs even at $\alpha = 0.7$, after significant performance deficits have emerged in both ResNet18 and ResNet20 (Appendix A.11). These findings rule out sparsity as a potential explanation for our results. The results are qualitatively similar for VGG16 (see Appendix A.12), indicating that increasing class selectivity beyond the levels that are learned naturally (i.e. without regularization, $\alpha = 0$) impairs network performance.

Recapitulation We directly compare the effects of increasing vs. decreasing class selectivity in Figure 4 (and Appendix A.15). The effects diverge immediately at $|\alpha| = 0.1$, and suppressing class selectivity yields a 6% increase in test accuracy relative to increasing class selectivity by $|\alpha| = 2.0$.

5 DISCUSSION

We examined the causal role of class selectivity in CNN performance by adding a term to the loss function that allows us to directly manipulate class selectivity across all neurons in the network. We found that class selectivity is not strictly necessary for networks to function, and that reducing it can even improve test accuracy. In ResNet18 trained on Tiny Imagenet, reducing class selectivity by $1.6 \times$ improved test accuracy by over 2%. In ResNet20 trained on CIFAR10, we could reduce the mean class selectivity of units in a network by factor of ~ 2.5 with no impact on test accuracy, and by a factor of ~ 20 —nearly to a mean of 0—with only a 2% change in test accuracy. We confirmed that our regularizer seems to suppress class selectivity, and not simply cause the network to rotate it off of unit-aligned axes. We also found that regularizing a network to increase class selectivity in individual units has negative effects on performance. These results resolve questions about class selectivity that remained inaccessible to previous approaches: class selectivity in individual units is neither necessary nor sufficient for—and can sometimes even constrain—CNN performance.

One caveat to our results is that they are limited to CNNs trained to perform image classification. It’s possible that our findings are due to idiosyncrasies of benchmark datasets, and wouldn’t generalize to more naturalistic datasets and tasks. Given that class selectivity is ubiquitous across DNNs trained on different tasks and datasets, future work should examine how broadly our results generalize, and the viability of class selectivity regularization as a general-purpose tool to improve DNN performance.

Our results make a broader point about the potential pitfalls of focusing on the properties of single units when trying to understand DNNs, emphasizing instead the importance of analyses that focus on *distributed* representations. While we consider it essential to find tractable, intuitive approaches for understanding complex systems, it's critical to empirically verify that these approaches actually reflect functionally relevant properties of the system being examined.

ACKNOWLEDGEMENTS

We would like to thank Tatiana Likhomanenko, Tiffany Cai, Eric Mintun, Janice Lan, Mike Rabbat, Sergey Edunov, Yuandong Tian, and Lyndon Duong for their productive scrutiny and insightful feedback.

REFERENCES

- E. D. Adrian. The impulses produced by sensory nerve endings. *The Journal of Physiology*, 61(1):49–72, March 1926. ISSN 0022-3751. URL <https://www.ncbi.nlm.nih.gov/pmc/articles/PMC1514809/>.
- Rana Ali Amjad, Kairen Liu, and Bernhard C. Geiger. Understanding Individual Neuron Importance Using Information Theory. April 2018. URL <https://arxiv.org/abs/1804.06679v3>.
- H B Barlow. Single Units and Sensation: A Neuron Doctrine for Perceptual Psychology? *Perception*, 1(4):371–394, December 1972. ISSN 0301-0066. doi: 10.1088/p010371. URL <https://doi.org/10.1088/p010371>.
- Anthony Bau, Yonatan Belinkov, Hassan Sajjad, Nadir Durrani, Fahim Dalvi, and James Glass. Identifying and Controlling Important Neurons in Neural Machine Translation. In *International Conference on Learning Representations*, 2019a. URL <https://openreview.net/forum?id=H1z-PsR5KX>.
- David Bau, Bolei Zhou, Aditya Khosla, Aude Oliva, and Antonio Torralba. Network Dissection: Quantifying Interpretability of Deep Visual Representations. In *2017 IEEE Conference on Computer Vision and Pattern Recognition (CVPR)*, pages 3319–3327, Honolulu, HI, July 2017. IEEE. ISBN 978-1-5386-0457-1. doi: 10.1109/CVPR.2017.354. URL <http://ieeexplore.ieee.org/document/8099837/>.
- David Bau, Jun-Yan Zhu, Hendrik Strobelt, Bolei Zhou, Joshua B. Tenenbaum, William T. Freeman, and Antonio Torralba. GAN Dissection: Visualizing and Understanding Generative Adversarial Networks. In *Proceedings of the International Conference on Learning Representations (ICLR)*, 2019b.
- David Bau, Jun-Yan Zhu, Hendrik Strobelt, Agata Lapedriza, Bolei Zhou, and Antonio Torralba. Understanding the role of individual units in a deep neural network. *Proceedings of the National Academy of Sciences*, September 2020. ISSN 0027-8424, 1091-6490. doi: 10.1073/pnas.1907375117. URL <https://www.pnas.org/content/early/2020/08/31/1907375117>. Publisher: National Academy of Sciences Section: Physical Sciences.
- Fahim Dalvi, Nadir Durrani, Hassan Sajjad, Yonatan Belinkov, Anthony Bau, and James Glass. What Is One Grain of Sand in the Desert? Analyzing Individual Neurons in Deep NLP Models. *Proceedings of the AAAI Conference on Artificial Intelligence*, 33(01):6309–6317, July 2019. ISSN 2374-3468. doi: 10.1609/aaai.v33i01.33016309. URL <https://aaai.org/ojs/index.php/AAAI/article/view/4592>.
- Kedar Dhamdhere, Mukund Sundararajan, and Qiqi Yan. How Important is a Neuron. In *International Conference on Learning Representations*, 2019. URL <https://openreview.net/forum?id=SylKoo0cKm>.
- Jonathan Donnelly and Adam Roegiest. On Interpretability and Feature Representations: An Analysis of the Sentiment Neuron. In Leif Azzopardi, Benno Stein, Norbert Fuhr, Philipp Mayr, Claudia Hauff, and Djoerd Hiemstra, editors, *Advances in Information Retrieval*, Lecture Notes in Computer Science, pages 795–802, Cham, 2019. Springer International Publishing. ISBN 978-3-030-15712-8. doi: 10.1007/978-3-030-15712-8_55.

Dumitru Erhan, Yoshua Bengio, Aaron C. Courville, and Pascal Vincent. Visualizing Higher-Layer Features of a Deep Network. 2009.

Li Fei-Fei, Andrej Karpathy, and Justin Johnson. Tiny imagenet visual recognition challenge, 2015. URL <https://tiny-imagenet.herokuapp.com/>.

Ruth Fong and Andrea Vedaldi. Net2Vec: Quantifying and Explaining How Concepts are Encoded by Filters in Deep Neural Networks. In *2018 IEEE/CVF Conference on Computer Vision and Pattern Recognition*, pages 8730–8738, Salt Lake City, UT, June 2018. IEEE. ISBN 978-1-5386-6420-9. doi: 10.1109/CVPR.2018.00910. URL <https://ieeexplore.ieee.org/document/8579008/>.

Stefano Fusi, Earl K. Miller, and Mattia Rigotti. Why neurons mix: high dimensionality for higher cognition. *Current opinion in neurobiology*, 37:66–74, 2016. doi: 10.1016/j.conb.2016.01.010. URL <http://eutils.ncbi.nlm.nih.gov/entrez/eutils/elink.fcgi?dbfrom=pubmed&id=26851755&retmode=ref&cmd=prlinks>.

Marianne Fyhn, Sturla Molden, Menno P. Witter, Edvard I. Moser, and May-Britt Moser. Spatial Representation in the Entorhinal Cortex. *Science*, 305(5688):1258–1264, August 2004. ISSN 0036-8075, 1095-9203. doi: 10.1126/science.1099901. URL <https://science.sciencemag.org/content/305/5688/1258>. Publisher: American Association for the Advancement of Science Section: Research Article.

Ella Gale, Ryan Blything, Nicholas Martin, Jeffrey S. Bowers, and Anh Nguyen. Selectivity metrics provide misleading estimates of the selectivity of single units in neural networks. In Ashok K. Goel, Colleen M. Seifert, and Christian Freksa, editors, *Proceedings of the 41th Annual Meeting of the Cognitive Science Society, CogSci 2019: Creativity + Cognition + Computation, Montreal, Canada, July 24-27, 2019*, pages 1808–1814. cognitivesciencesociety.org, 2019. URL <https://mindmodeling.org/cogsci2019/papers/0319/index.html>.

Juan A. Gallego, Matthew G. Perich, Stephanie N. Naufel, Christian Ethier, Sara A. Solla, and Lee E. Miller. Cortical population activity within a preserved neural manifold underlies multiple motor behaviors. *Nature Communications*, 9(1):4233, December 2018. ISSN 2041-1723. doi: 10.1038/s41467-018-06560-z. URL <http://www.nature.com/articles/s41467-018-06560-z>.

Ragnar Granit. *Receptors and sensory perception*. Receptors and sensory perception. Yale University Press, New Haven, CT, US, 1955.

Kaiming He, Xiangyu Zhang, Shaoqing Ren, and Jian Sun. Deep residual learning for image recognition. In *Proceedings of the IEEE conference on computer vision and pattern recognition*, pages 770–778, 2016.

David J. Heeger and Wayne E. Mackey. Oscillatory recurrent gated neural integrator circuits (organics), a unifying theoretical framework for neural dynamics. *Proceedings of the National Academy of Sciences*, 116(45):22783–22794, 2019. ISSN 0027-8424. doi: 10.1073/pnas.1911633116. URL <https://www.pnas.org/content/116/45/22783>.

Sara Hooker, Dumitru Erhan, Pieter-Jan Kindermans, and Been Kim. A Benchmark for Interpretability Methods in Deep Neural Networks. In H. Wallach, H. Larochelle, A. Beygelzimer, F. Alché-Buc, E. Fox, and R. Garnett, editors, *Advances in Neural Information Processing Systems 32*, pages 9734–9745. Curran Associates, Inc., 2019. URL <http://papers.nips.cc/paper/9167-a-benchmark-for-interpretability-methods-in-deep-neural-networks.pdf>.

Harold Hotelling. Relations Between Two Sets of Variates. *Biometrika*, 28(3/4):321–377, 1936. ISSN 0006-3444. doi: 10.2307/2333955. URL <https://www.jstor.org/stable/2333955>.

D. H. Hubel and T. N. Wiesel. Receptive fields of single neurones in the cat’s striate cortex. *The Journal of Physiology*, 148(3):574–591, 1959. ISSN 1469-7793. doi: 10.1113/jphysiol.1959.sp006308. URL <https://physoc.onlinelibrary.wiley.com/doi/abs/10.1113/jphysiol.1959.sp006308>.

-
- D. H. Hubel and T. N. Wiesel. Receptive fields, binocular interaction and functional architecture in the cat’s visual cortex. *The Journal of Physiology*, 160(1):106–154, 1962. ISSN 1469-7793. doi: 10.1113/jphysiol.1962.sp006837. URL <https://physoc.onlinelibrary.wiley.com/doi/abs/10.1113/jphysiol.1962.sp006837>.
- David H. Hubel. Exploration of the primary visual cortex, 1955–78. *Nature*, 299(5883):515–524, October 1982. ISSN 1476-4687. doi: 10.1038/299515a0. URL <https://www.nature.com/articles/299515a0>.
- Yerlan Idelbayev. akamaster/pytorch_resnet_cifar10, January 2020. URL https://github.com/akamaster/pytorch_resnet_cifar10. original-date: 2018-01-15T09:50:56Z.
- Michele N Insanally, Ioana Carcea, Rachel E Field, Chris C Rodgers, Brian DePasquale, Kanaka Rajan, Michael R DeWeese, Badr F Albanna, and Robert C Froemke. Spike-timing-dependent ensemble encoding by non-classically responsive cortical neurons. *eLife*, 8:e42409, January 2019. ISSN 2050-084X. doi: 10.7554/eLife.42409. URL <https://doi.org/10.7554/eLife.42409>.
- Yuta Kanda, Kota S. Sasaki, Izumi Ohzawa, and Hiroshi Tamura. Deleting object selective units in a fully-connected layer of deep convolutional networks improves classification performance. *arXiv:2001.07811 [q-bio]*, January 2020. URL <http://arxiv.org/abs/2001.07811>. arXiv: 2001.07811.
- E R Kandel, J H Schwartz, and Jessica Chao. *Principles of neural science*. McGraw-Hill, New York, 2000.
- Andrej Karpathy, Justin Johnson, and Li Fei-Fei. Visualizing and Understanding Recurrent Networks. In *International Conference on Learning Representations*, page 11, 2016.
- Diederik P. Kingma and Jimmy Ba. Adam: A method for stochastic optimization. In Yoshua Bengio and Yann LeCun, editors, *3rd International Conference on Learning Representations, ICLR 2015, San Diego, CA, USA, May 7-9, 2015, Conference Track Proceedings*, 2015. URL <http://arxiv.org/abs/1412.6980>.
- Alex Krizhevsky. Learning Multiple Layers of Features from Tiny Images. Technical report, 2009.
- Matthew L Leavitt, Florian Pieper, Adam J Sachs, and Julio C Martinez-Trujillo. Correlated variability modifies working memory fidelity in primate prefrontal neuronal ensembles. *Proceedings of the National Academy of Sciences of the United States of America*, 114(12):E2494–E2503, 2017. doi: 10.1073/pnas.1619949114. URL <http://www.pnas.org/lookup/doi/10.1073/pnas.1619949114>.
- Mario Lezcano-Casado. Trivializations for gradient-based optimization on manifolds. In *Advances in Neural Information Processing Systems, NeurIPS*, pages 9154–9164, 2019.
- Yixuan Li, Jason Yosinski, Jeff Clune, Hod Lipson, and John Hopcroft. Convergent learning: Do different neural networks learn the same representations? In Dmitry Storcheus, Afshin Rostamizadeh, and Sanjiv Kumar, editors, *Proceedings of the 1st International Workshop on Feature Extraction: Modern Questions and Challenges at NIPS 2015*, volume 44 of *Proceedings of Machine Learning Research*, pages 196–212, Montreal, Canada, 11 Dec 2015. PMLR. URL <http://proceedings.mlr.press/v44/li15convergent.html>.
- Peter E. Lillian, Richard Meyes, and Tobias Meisen. Ablation of a Robot’s Brain: Neural Networks Under a Knife. December 2018. URL <https://arxiv.org/abs/1812.05687v2>.
- Lu Lu, Yeonjong Shin, Yanhui Su, and George Em Karniadakis. Dying ReLU and Initialization: Theory and Numerical Examples. *arXiv:1903.06733 [cs, math, stat]*, November 2019. URL <http://arxiv.org/abs/1903.06733>. arXiv: 1903.06733.
- Andrew L. Maas, Awni Y. Hannun, and Andrew Y. Ng. Rectifier nonlinearities improve neural network acoustic models. In *ICML Workshop on Deep Learning for Audio, Speech and Language Processing*, 2013.

Richard Meyes, Melanie Lu, Constantin Waubert de Puiseau, and Tobias Meisen. Ablation Studies in Artificial Neural Networks. [arXiv:1901.08644 \[cs, q-bio\]](https://arxiv.org/abs/1901.08644), February 2019. URL <http://arxiv.org/abs/1901.08644>. arXiv: 1901.08644.

Sohie Lee Moody, Steven P. Wise, Giuseppe di Pellegrino, and David Zipser. A Model That Accounts for Activity in Primate Frontal Cortex during a Delayed Matching-to-Sample Task. *Journal of Neuroscience*, 18(1):399–410, January 1998. ISSN 0270-6474, 1529-2401. doi: 10.1523/JNEUROSCI.18-01-00399.1998. URL <https://www.jneurosci.org/content/18/1/399>.

Ari Morcos, Maithra Raghu, and Samy Bengio. Insights on representational similarity in neural networks with canonical correlation. In S. Bengio, H. Wallach, H. Larochelle, K. Grauman, N. Cesa-Bianchi, and R. Garnett, editors, *Advances in Neural Information Processing Systems 31*, pages 5727–5736. Curran Associates, Inc., 2018a. URL [http://papers.nips.cc/paper/7815-insights-on-representational-similarity-in-neural-networks-with-canonical-correlation.pdf](https://papers.nips.cc/paper/7815-insights-on-representational-similarity-in-neural-networks-with-canonical-correlation.pdf).

Ari S. Morcos and Christopher D. Harvey. History-dependent variability in population dynamics during evidence accumulation in cortex. *Nature Neuroscience*, 19(12):1672–1681, December 2016. ISSN 1546-1726. doi: 10.1038/nn.4403. URL <https://www.nature.com/articles/nn.4403>.

Ari S. Morcos, David G. T. Barrett, Neil C. Rabinowitz, and Matthew Botvinick. On the importance of single directions for generalization. In *International Conference on Learning Representations*, 2018b. URL <https://openreview.net/forum?id=r1iuQjxZ>.

Seil Na, Yo Joong Choe, Dong-Hyun Lee, and Gunhee Kim. Discovery of Natural Language Concepts in Individual Units of CNNs. In *International Conference on Learning Representations*, 2019. URL <https://openreview.net/forum?id=S1EERs09YQ>.

Anh Nguyen, Alexey Dosovitskiy, Jason Yosinski, Thomas Brox, and Jeff Clune. Synthesizing the preferred inputs for neurons in neural networks via deep generator networks. In D. D. Lee, M. Sugiyama, U. V. Luxburg, I. Guyon, and R. Garnett, editors, *Advances in Neural Information Processing Systems 29*, pages 3387–3395. Curran Associates, Inc., 2016. URL [http://papers.nips.cc/paper/6519-synthesizing-the-preferred-inputs-for-neurons-in-neural-networks-via-deep-generator-networks.pdf](https://papers.nips.cc/paper/6519-synthesizing-the-preferred-inputs-for-neurons-in-neural-networks-via-deep-generator-networks.pdf).

J. O’Keefe and J. Dostrovsky. The hippocampus as a spatial map. Preliminary evidence from unit activity in the freely-moving rat. *Brain Research*, 34(1):171–175, November 1971. ISSN 0006-8993. doi: 10.1016/0006-8993(71)90358-1. URL <https://www.sciencedirect.com/science/article/pii/0006899371903581>.

Chris Olah, Alexander Mordvintsev, and Ludwig Schubert. Feature Visualization. *Distill*, 2(11):e7, November 2017. ISSN 2476-0757. doi: 10.23915/distill.00007. URL <https://distill.pub/2017/feature-visualization>.

Chris Olah, Arvind Satyanarayan, Ian Johnson, Shan Carter, Ludwig Schubert, Katherine Ye, and Alexander Mordvintsev. The Building Blocks of Interpretability. *Distill*, 3(3):e10, March 2018. ISSN 2476-0757. doi: 10.23915/distill.00010. URL <https://distill.pub/2018/building-blocks>.

Chris Olah, Nick Cammarata, Ludwig Schubert, Gabriel Goh, Michael Petrov, and Shan Carter. Zoom In: An Introduction to Circuits. *Distill*, 5(3):e00024.001, March 2020. ISSN 2476-0757. doi: 10.23915/distill.00024.001. URL <https://distill.pub/2020/circuits/zoom-in>.

Adam Paszke, Sam Gross, Francisco Massa, Adam Lerer, James Bradbury, Gregory Chanan, Trevor Killeen, Zeming Lin, Natalia Gimelshein, Luca Antiga, Alban Desmaison, Andreas Kopf, Edward Yang, Zachary DeVito, Martin Raison, Alykhan Tejani, Sasank Chilamkurthy, Benoit Steiner, Lu Fang, Junjie Bai, and Soumith Chintala. PyTorch: An Imperative Style, High-Performance Deep Learning Library. In H. Wallach, H. Larochelle, A. Beygelzimer, F. d’Alché-Buc, E. Fox, and R. Garnett, editors, *Advances in Neural Information Processing Systems 32*, pages 8024–8035. Curran Associates, Inc.,

-
2019. URL <http://papers.neurips.cc/paper/9015-pytorch-an-imperative-style-high-performance-deep-learning-library.pdf>.
- J Andrew Pruszynski and Joel Zylberberg. The language of the brain: real-world neural population codes. *Current Opinion in Neurobiology*, 58:30–36, October 2019. ISSN 09594388. doi: 10.1016/j.conb.2019.06.005. URL <https://linkinghub.elsevier.com/retrieve/pii/S0959438818302137>.
- Alec Radford, Rafal Jozefowicz, and Ilya Sutskever. Learning to Generate Reviews and Discovering Sentiment. *arXiv:1704.01444 [cs]*, April 2017. URL <http://arxiv.org/abs/1704.01444>. arXiv: 1704.01444.
- Ivet Rafeagas, Maria Vanrell, Luis A. Alexandre, and Guillem Arias. Understanding trained CNNs by indexing neuron selectivity. *Pattern Recognition Letters*, page S0167865519302909, October 2019. ISSN 01678655. doi: 10.1016/j.patrec.2019.10.013. URL <http://arxiv.org/abs/1702.00382>. arXiv: 1702.00382.
- Maithra Raghu, Justin Gilmer, Jason Yosinski, and Jascha Sohl-Dickstein. SVCCA: Singular Vector Canonical Correlation Analysis for Deep Learning Dynamics and Interpretability. In I. Guyon, U. V. Luxburg, S. Bengio, H. Wallach, R. Fergus, S. Vishwanathan, and R. Garnett, editors, *Advances in Neural Information Processing Systems 30*, pages 6076–6085. Curran Associates, Inc., 2017.
- David Raposo, Matthew T Kaufman, and Anne K Churchland. A category-free neural population supports evolving demands during decision-making. *Nature Neuroscience*, 17(12):1784–1792, 2014. doi: 10.1038/nn.3865. URL <http://eutils.ncbi.nlm.nih.gov/entrez/eutils/elink.fcgi?dbfrom=pubmed&id=25383902&retmode=ref&cmd=prlinks>.
- Shreya Saxena and John P Cunningham. Towards the neural population doctrine. *Current Opinion in Neurobiology*, 55:103–111, April 2019. ISSN 0959-4388. doi: 10.1016/j.conb.2019.02.002. URL <http://www.sciencedirect.com/science/article/pii/S0959438818300990>.
- Krishna V Shenoy, Maneesh Sahani, and Mark M Churchland. Cortical control of arm movements: a dynamical systems perspective. *Annual Review of Neuroscience*, 36:337–359, 2013. doi: 10.1146/annurev-neuro-062111-150509. URL <http://eutils.ncbi.nlm.nih.gov/entrez/eutils/elink.fcgi?dbfrom=pubmed&id=23725001&retmode=ref&cmd=prlinks>.
- Charles S. Sherrington. *The integrative action of the nervous system*. The integrative action of the nervous system. Yale University Press, New Haven, CT, US, 1906. doi: 10.1037/13798-000.
- Karen Simonyan and Andrew Zisserman. Very deep convolutional networks for large-scale image recognition. In Yoshua Bengio and Yann LeCun, editors, *3rd International Conference on Learning Representations, ICLR 2015, San Diego, CA, USA, May 7-9, 2015, Conference Track Proceedings*, 2015. URL <http://arxiv.org/abs/1409.1556>.
- Karen Simonyan, Andrea Vedaldi, and Andrew Zisserman. Deep Inside Convolutional Networks: Visualising Image Classification Models and Saliency Maps. *arXiv:1312.6034 [cs]*, April 2014. URL <http://arxiv.org/abs/1312.6034>. arXiv: 1312.6034.
- Stephen M. Smith, Thomas E. Nichols, Diego Vidaurre, Anderson M. Winkler, Timothy E. J. Behrens, Matthew F. Glasser, Kamil Ugurbil, Deanna M. Barch, David C. Van Essen, and Karla L. Miller. A positive-negative mode of population covariation links brain connectivity, demographics and behavior. *Nature Neuroscience*, 18(11):1565–1567, November 2015. ISSN 1546-1726. doi: 10.1038/nn.4125. URL <https://www.nature.com/articles/nn.4125>.
- David Sussillo, Mark M Churchland, Matthew T Kaufman, and Krishna V Shenoy. A neural network that finds a naturalistic solution for the production of muscle activity. *Nature Neuroscience*, 18(7):1025–1033, 2015. doi: 10.1038/nn.4042. URL <http://eutils.ncbi.nlm.nih.gov/entrez/eutils/elink.fcgi?dbfrom=pubmed&id=26075643&retmode=ref&cmd=prlinks>.

Jumpei Ukita. Causal importance of orientation selectivity for generalization in image recognition. September 2018. URL https://openreview.net/forum?id=Bkx_Dj09tQ.

Pauli Virtanen, Ralf Gommers, Travis E. Oliphant, Matt Haberland, Tyler Reddy, David Cournapeau, Evgeni Burovski, Pearu Peterson, Warren Weckesser, Jonathan Bright, Stéfan J. van der Walt, Matthew Brett, Joshua Wilson, K. Jarrod Millman, Nikolay Mayorov, Andrew R. J. Nelson, Eric Jones, Robert Kern, Eric Larson, C. J. Carey, Ilhan Polat, Yu Feng, Eric W. Moore, Jake VanderPlas, Denis Laxalde, Josef Perktold, Robert Cimrman, Ian Henriksen, E. A. Quintero, Charles R. Harris, Anne M. Archibald, Antônio H. Ribeiro, Fabian Pedregosa, Paul van Mulbregt, and SciPy 1.0 Contributors. SciPy 1.0—Fundamental Algorithms for Scientific Computing in Python. [arXiv:1907.10121 \[physics\]](https://arxiv.org/abs/1907.10121), July 2019. URL <http://arxiv.org/abs/1907.10121>. arXiv: 1907.10121.

Michael Waskom, Olga Botvinnik, Drew O’Kane, Paul Hobson, Saulius Lukauskas, David C. Gemperline, Tom Augspurger, Yaroslav Halchenko, John B. Cole, Jordi Warmenhoven, Julian de Ruiter, Cameron Pye, Stephan Hoyer, Jake Vanderplas, Santi Villalba, Gero Kunter, Eric Quintero, Pete Bachant, Marcel Martin, Kyle Meyer, Alistair Miles, Yoav Ram, Tal Yarkoni, Mike Lee Williams, Constantine Evans, Clark Fitzgerald, Brian, Chris Fonnesbeck, Antony Lee, and Adel Qalieh. mwaskom/seaborn: v0.8.1 (September 2017), September 2017. URL <https://doi.org/10.5281/zenodo.883859>.

T. N. Wiesel. Postnatal development of the visual cortex and the influence of environment. *Nature*, 299(5884):583–591, October 1982. ISSN 0028-0836. doi: 10.1038/299583a0.

Jason Yosinski, Jeff Clune, Anh Nguyen, Thomas Fuchs, and Hod Lipson. Understanding Neural Networks Through Deep Visualization. In *ICML Workshop on Visualization for Deep Learning*, 2015. URL [http://arxiv.org/abs/1506.06579](https://arxiv.org/abs/1506.06579). arXiv: 1506.06579.

Matthew D. Zeiler and Rob Fergus. Visualizing and Understanding Convolutional Networks. In David Fleet, Tomas Pajdla, Bernt Schiele, and Tinne Tuytelaars, editors, *Computer Vision – ECCV 2014*, pages 818–833, Cham, 2014. Springer International Publishing. ISBN 978-3-319-10590-1.

B. Zhou, D. Bau, A. Oliva, and A. Torralba. Interpreting Deep Visual Representations via Network Dissection. *IEEE Transactions on Pattern Analysis and Machine Intelligence*, 41(9):2131–2145, September 2019. ISSN 1939-3539. doi: 10.1109/TPAMI.2018.2858759.

Bolei Zhou, Aditya Khosla, Agata Lapedriza, Aude Oliva, and Antonio Torralba. Object Detectors Emerge in Deep Scene CNNs. In *International Conference on Learning Representations*, April 2015. URL [http://arxiv.org/abs/1412.6856](https://arxiv.org/abs/1412.6856). arXiv: 1412.6856.

Bolei Zhou, Yiyou Sun, David Bau, and Antonio Torralba. Revisiting the Importance of Individual Units in CNNs via Ablation. [arXiv:1806.02891 \[cs\]](https://arxiv.org/abs/1806.02891), June 2018. URL <http://arxiv.org/abs/1806.02891>. arXiv: 1806.02891.

Joel Zylberberg. The role of untuned neurons in sensory information coding. *bioRxiv*, page 134379, May 2018. doi: 10.1101/134379. URL <https://www.biorxiv.org/content/10.1101/134379v6>.

A APPENDIX

A.1 MODELS, TRAINING, DATASETS, AND SOFTWARE

Our experiments were performed on ResNet18 (He et al., 2016) trained on Tiny Imagenet (Fei-Fei et al., 2015), and ResNet20 (He et al. (2016); code modified from Idelbayev (2020)) and a VGG16-like network (Simonyan and Zisserman, 2015), both trained on CIFAR10 (Krizhevsky, 2009). All models were trained using stochastic gradient descent (SGD) with momentum = 0.9 and weight decay = 0.0001.

The maxpool layer after the first batchnorm layer (see He et al. (2016)) was removed because of the smaller size of Tiny Imagenet images compared to standard ImageNet images (64x64 vs. 256x256, respectively). ResNet18 were trained for 90 epochs with a minibatch size of 4096 samples with a learning rate of 0.1, multiplied (annealed) by 0.1 at epochs 35, 50, 65, and 80. Tiny Imagenet (Fei-Fei et al., 2015) consists of 500 training images and 50 images for each of its 200 classes. We used the validation set for testing and created a new validation set by taking 50 images per class from the training set, selected randomly for each training run.

The VGG16-like network is identical to the batch norm VGG16 in Simonyan and Zisserman (2015), except the final two fully-connected layers of 4096 units each were replaced with a single 512-unit layer. ResNet20 and VGG16 were trained for 200 epochs using a minibatch size of 256 samples. ResNet20 were trained with a learning rate of 0.1 and VGG16 with a learning rate of 0.01, both annealed by 10^{-1} at epochs 100 and 150. We split the 50k CIFAR10 training samples into a 45k sample training set and a 5k validation set, similar to our approach with Tiny Imagenet.

All experimental results were derived from the test set with the parameters from the epoch that achieved the highest validation set accuracy over the training epochs. 20 replicates with different random seeds were run for each hyperparameter set. Selectivity regularization was not applied to the final (output) layer, nor was the final layer included any of our analyses.

Experiments were conducted using PyTorch (Paszke et al., 2019), analyzed using the SciPy ecosystem (Virtanen et al., 2019), and visualized using Seaborn (Waskom et al., 2017).

A.2 EFFECT OF SELECTIVITY REGULARIZER ON TRAINING TIME

We quantified the number of training epochs required to reach 95% of maximum test accuracy (t^{95}). The t^{95} without selectivity regularization ($t_{\alpha=0}^{95}$) for ResNet20 is 45 ± 15 epochs (median \pm IQR). α in [-2, 0.7] had overlapping IQRs with $\alpha = 0$. For ResNet18, $t_{\alpha=0}^{95} = 35 \pm 1$, while t^{95} for α in [-2, 1] was as high as 51 ± 1.5 . Beyond these ranges, the t^{95} exceeded $1.5 \times t_{\alpha=0}^{95}$ and/or was highly variable.

A.3 CCA

A.3.1 AN INTUITION

We used Canonical Correlation Analysis (CCA) to examine the effects of class selectivity regularization on hidden layer representations. CCA is a statistical method that takes two sets of multidimensional variates and finds the linear combinations of these variates that have maximum correlation with each other (Hotelling, 1936). Critically, CCA is invariant to rotation and other invertible affine transformations. CCA has been productively applied to analyze and compare representations in (and between) biological and neural networks (Sussillo et al., 2015; Smith et al., 2015; Raghu et al., 2017; Morcos et al., 2018a; Gallego et al., 2018).

We use projection-weighted CCA (PWCCA), a variant of CCA introduced in Morcos et al. (2018a) that has been shown to be more robust to noise than traditional CCA and other CCA variants (though for brevity we just use the term "CCA" in the main text). PWCCA generates a scalar value, ρ , that can be thought of as the distance or dissimilarity between the two sets of multidimensional variates, L_1 and L_2 . For example, if $L_2 = L_1$, then $\rho_{L_1, L_2} = 0$. Now let R be a rotation matrix. Because CCA is invariant to rotation and other invertible affine transformations, if $L_2 = RL_1$ (i.e. if L_2 is a rotation of L_1), then $\rho_{L_1, L_2} = 0$. In contrast, traditional similarity metrics such as Pearson's Correlation and cosine similarity would obtain different values if $L_2 = L_1$ compared to $L_2 = RL_1$.

We use the PWCCA implementation available at <https://github.com/google/svcca/>, as provided in Morcos et al. (2018a).

A.3.2 OUR APPLICATION

As an example for the analyses in our experiments, L_1 is the activation matrix for a layer in a network that was not regularized against class selectivity (i.e. $\alpha = 0$), and L_2 is the activation matrix for the same layer in a network that was structured and initialized identically, but subject to regularization against class selectivity (i.e. $\alpha < 0$). If regularizing against class selectivity causes the network’s representations to be rotated (or to undergo to some other invertible affine transformation), then $\rho_{L_1, L_2} = 0$. In practice $\rho_{L_1, L_2} > 0$ due to differences in random seeds and/or other stochastic factors in the training process, so we can determine a threshold value ϵ and say $\rho_{L_1, L_2} \leq \epsilon$. If regularizing against class selectivity instead causes a non-affine transformation to the network’s representations, then $\rho_{L_1, L_2} > \epsilon$.

In our experiments we empirically establish a distribution of ϵ values by computing the PWCCA distances between $\rho_{L_{2a} L_{2b}}$, where L_{2a} and L_{2b} are two networks from the set of 20 replicates for a given hyperparameter combination that differ only in their initial random seed values (and thus have the same α). This gives $\binom{20}{2} = 190$ values of ϵ . We then compute the PWCCA distance between each $\{L_1, L_2\}$ replicate pair, yielding a distribution of $20 \times 20 = 400$ values of ρ_{L_1, L_2} , which we compare to the distribution of ϵ .

A.3.3 FORMALLY

For the case of our analyses, let us start with a dataset X , which consists of M data samples $\{x_1, \dots, x_M\}$. Using the notation from Raghu et al. (2017), the scalar output (activation) of a single neuron i on layer ι in response to each data sample collectively form the vector

$$z_i^\iota = (z(x_i^\iota(x_1), \dots, x_i^\iota(x_M)))$$

We then collect the activation vector z_i^ι of every neuron in layer ι into a matrix $L = \{z_1^\iota, \dots, z_M^\iota\}$ of size $N \times M$, N is the number of neurons in layer ι , and M is the number of data samples. Given two such activation matrices L_1 , of size $N_a \times M$, and L_2 , of size $N_b \times M$, CCA finds the vectors w (in \mathbb{R}^{N_a}) and s (in \mathbb{R}^{N_b}), such that the inner product

$$\rho = 1 - \frac{\langle w^T L_1, s^T L_2 \rangle}{\|w^T L_1\| \cdot \|s^T L_2\|}$$

is maximized.

A.4 REGULARIZING TO DECREASE CLASS SELECTIVITY IN RESNET18 AND RESNET20

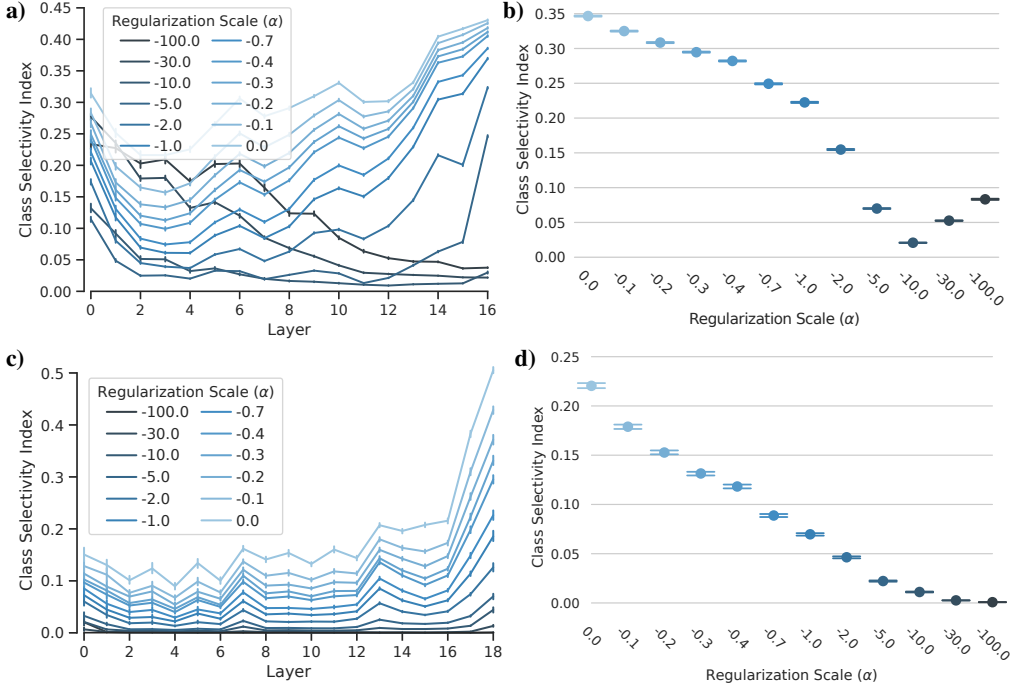


Figure A1: Manipulating class selectivity by regularizing against it in the loss function. (a) Mean class selectivity index (y-axis) as a function of layer (x-axis) for different regularization scales (α ; denoted by intensity of blue) for ResNet18. (b) Similar to (a), but mean is computed across all units in a network instead of per layer. (c) Similar to (a), but mean is computed across all units in a network instead of per layer. (d) are identical to (a) and (b), respectively, but for ResNet20. Error bars denote bootstrapped 95% confidence intervals.

A.5 DECREASING CLASS SELECTIVITY WITHOUT DECREASING TEST ACCURACY IN RESNET20

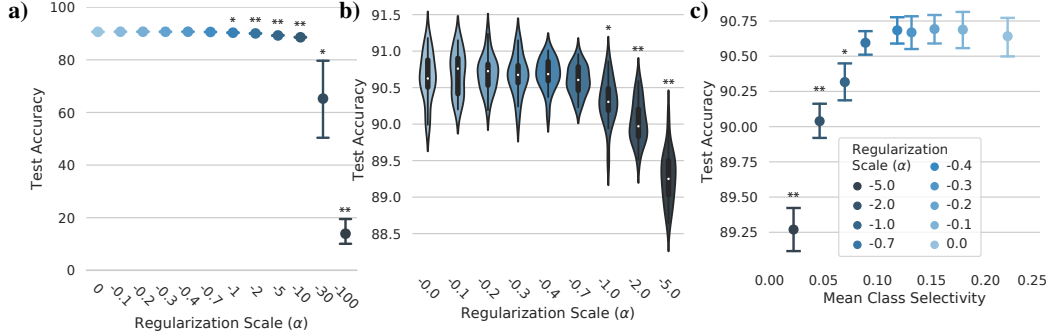


Figure A2: Effects of reducing class selectivity on test accuracy in ResNet20 trained on CIFAR10. (a) Test accuracy (y-axis) as a function of regularization scale (α , x-axis and intensity of blue). (b) Identical to (a), but for a subset of α values. The center of each violin plot contains a boxplot, in which the darker central lines denote the central two quartiles. (c) Test accuracy (y-axis) as a function of mean class selectivity (x-axis) for different values of α . Error bars denote 95% confidence intervals. * $p < 0.05$, ** $p < 5 \times 10^{-6}$ difference from $\alpha = 0$, t-test, Bonferroni-corrected.

A.6 CCA RESULTS FOR RESNET20

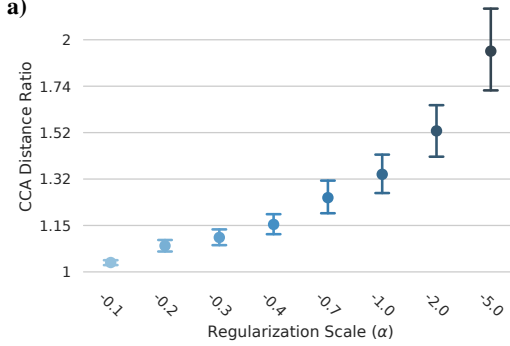


Figure A3: Using CCA to check whether class selectivity is rotated off-axis in ResNet20 trained on CIFAR10. Similar to Figure 2, we plot the average CCA distance ratio (y-axis) as a function of α (x-axis, intensity of blue). The distance ratio is significantly greater than the baseline for all values of α ($p < 5 \times 10^{-6}$, paired t-test). Error bars = 95% confidence intervals.

A.7 CALCULATING AN UPPER BOUND FOR OFF-AXIS SELECTIVITY

As an additional control to ensure that our regularizer did not simply shift class selectivity to off-axis directions in activation space, we calculated an upper bound on the amount of class selectivity that could be recovered by finding the linear projection of unit activations that maximizes class selectivity. To do so, we first collected the validation set activation vector z_i^l of every neuron in layer l into a matrix $A_{val} = \{z_1^l, \dots, z_M^l\}$ of size $M \times N$, where M is the number of data samples in validation set and N is the number of neurons in layer l . We then found the projection matrix $W \in \mathbb{R}^{N \times N}$ that minimizes the loss

$$loss = (1 - SI(A_{val}W))$$

such that

$$\|W^T W - I\|^2 = 0$$

i.e. W is orthonormal, where SI is the selectivity index from Equation 1. We constrained W to be orthonormal using Lezcano-Casado (2019)'s toolbox. Because SI requires inputs ≥ 0 , we shifted the columns of AW by subtracting the columnwise minimum value before computing SI . The optimization was performed using Adam (Kingma and Ba, 2015) with a learning rate of 0.001 for 3500 steps or until the magnitude of the change in loss was less than 10^{-6} for 10 steps. W was then used to project the activation matrix for the test set A_{test} , and the selectivity index was calculated for each axis of the new activation space (i.e. each column of $A_{test}W$) after shifting the columns of $A_{test}W$ to be ≥ 0 . A separate W was obtained for each layer of each model and for each replicate and value of α .

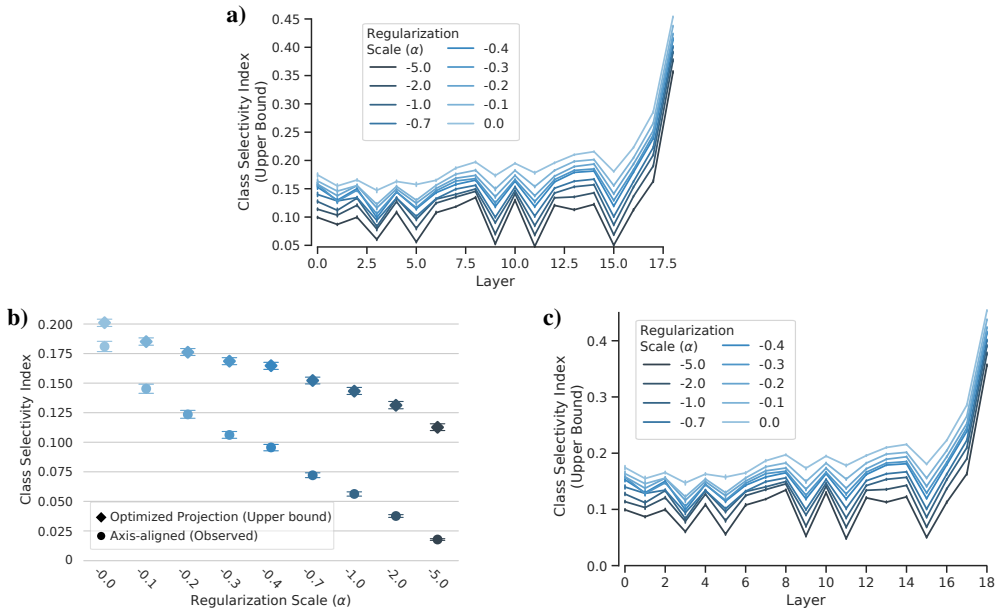


Figure A4: An upper bound for off-axis class selectivity. (a) Upper bound on class selectivity (y-axis) as a function of layer (x-axis) for different regularization scales (α ; denoted by intensity of blue) for ResNet18 trained on Tiny ImageNet. (b) Mean class selectivity (y-axis) as a function of regularization scale (α ; x-axis) for ResNet20 trained on CIFAR10. Diamond-shaped data points denote the upper bound on class selectivity for a linear projection of activations as described in Appendix A.7, while circular points denote the amount of axis-aligned class selectivity for the corresponding values of α . (c) (a), but for ResNet20 trained on CIFAR10. Error bars = 95% confidence intervals.

A.8 REGULARIZING TO INCREASE CLASS SELECTIVITY IN RESNET18 AND RESNET20

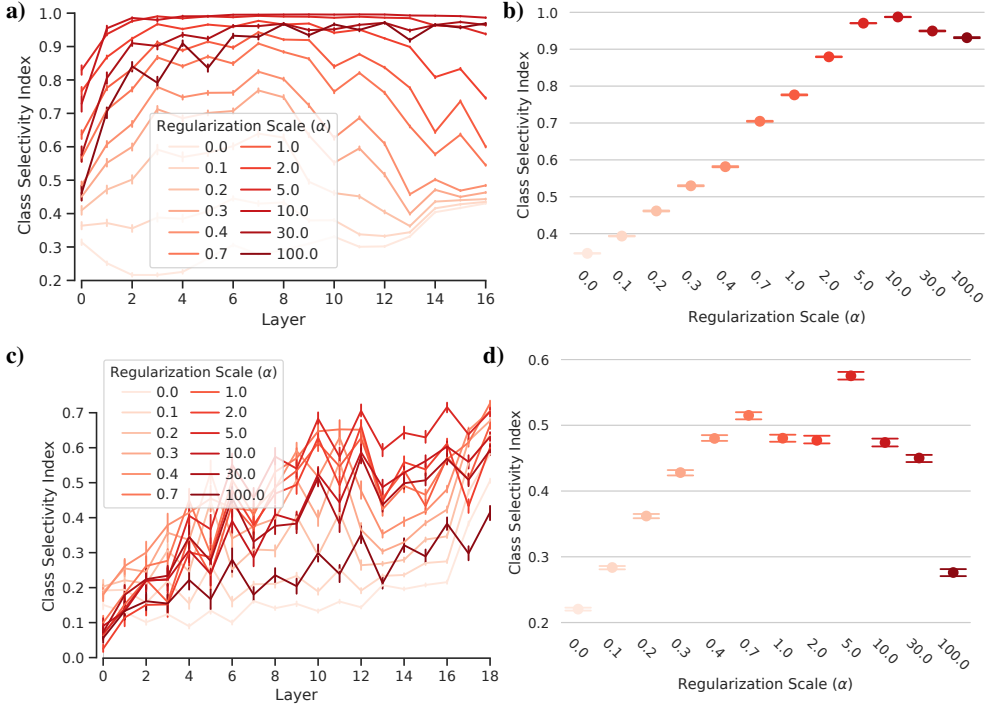


Figure A5: Regularizing to increase class selectivity **(a)** Mean class selectivity index (y-axis) as a function of layer (x-axis) for different regularization scales (α ; denoted by intensity of red) for ResNet18. **(b)** Similar to **(a)**, but mean is computed across all units in a network instead of per layer. **(c)** and **(d)** are identical to **(a)** and **(b)**, respectively, but for ResNet20. Note that the inconsistent effect of larger α values in **(c)** and **(d)** is addressed in Appendix A.10. Error bars denote bootstrapped 95% confidence intervals.

A.9 INCREASED CLASS SELECTIVITY IMPAIRS TEST ACCURACY IN RESNET20

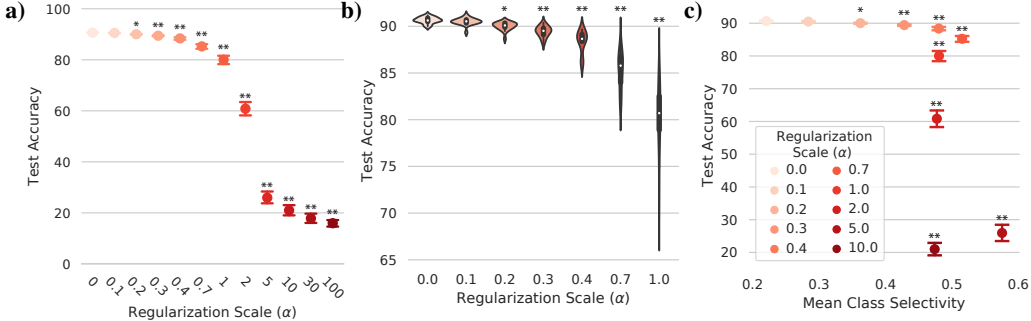


Figure A6: Effects of increasing class selectivity on test accuracy on ResNet20 trained on CIFAR10. (a) Test accuracy (y-axis) as a function of regularization scale (α ; x-axis, intensity of red). (b) Identical to (a), but for a subset of α values. The center of each violin plot contains a boxplot, in which the darker central lines denote the central two quartiles. (c) Test accuracy (y-axis) as a function of mean class selectivity (x-axis) for different values of α . Error bars denote 95% confidence intervals. $*p < 2 \times 10^{-4}$, $**p < 5 \times 10^{-7}$ difference from $\alpha = 0$, t-test, Bonferroni-corrected.

A.10 SINGLE UNIT NECROMANCY

Lethal ReLUs The inconsistent relationship between α and class selectivity for larger values of α led us to question whether the performance deficits were due to an alternative factor, such as the optimization process, rather than class selectivity per se. Interestingly, we observed that ResNet20 regularized to increase selectivity contained significantly higher proportions of dead units, and the number of dead units is roughly proportional to alpha (see Figure A7a; also note that this was not a problem in ResNet18). Removing the dead units makes the relationship between regularization and selectivity in ResNet20 more consistent at large regularization scales (see Appendix A7).

The presence of dead units is not unexpected, as units with the ReLU activation function are known to suffer from the "dying ReLU problem" (Lu et al., 2019): If, during training, a weight update causes a unit to cease activating in response to all training samples, the unit will be unaffected by subsequent weight updates because the ReLU gradient at $x \leq 0$ is zero, and thus the unit's activation will forever remain zero. The dead units could explain the decrease in performance from regularizing to increase selectivity as simply a decrease in model capacity.

Fruitless resuscitation One solution to the dying ReLU problem is to use a leaky-ReLU activation function (Maas et al., 2013), which has a non-zero slope, b (and thus non-zero gradient) for $x \leq 0$. Accordingly, we re-ran the previous experiment using units with a leaky-ReLU activation in an attempt to control for the potential confound of dead units. Note that because the class selectivity index assumes activations ≥ 0 , we shifted activations by subtracting the minimum activation when computing selectivity for leaky-ReLUs. If the performance deficits from regularizing for selectivity are simply due to dead units, then using leaky-ReLUs should rescue performance. Alternatively, if dead units are not the cause of the performance deficits, then leaky-ReLUs should not have an effect.

We first confirmed that using leaky-ReLUs solves the dead unit problem. Indeed, the proportion of dead units is reduced to 0 in all networks across all tested values of b . Despite complete recovery of the dead units, however, using leaky-ReLUs does not rescue class selectivity-induced performance deficits (Figure A8). While the largest negative slope value improved test accuracy for larger values of α , the improvement was minor, and increasing α still had catastrophic effects. These results confirm that dead units cannot explain the rapid and catastrophic effects of increased class selectivity on performance.

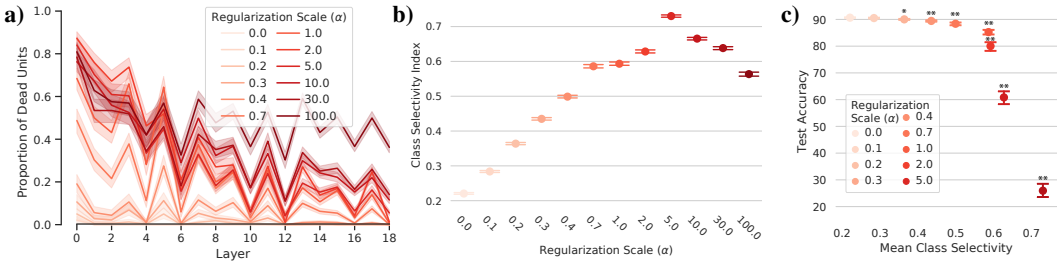


Figure A7: Removing dead units partially stabilizes the effects of large positive regularization scales in ResNet20. (a) Proportion of dead units (y-axis) as a function of layer (x-axis) for different regularization scales (α ; intensity of red). (b) Mean class selectivity index (y-axis) as a function of regularization scale (α ; x-axis and intensity of red) after removing dead units. Removing dead units from the class selectivity calculation establishes a more consistent relationship between α and the mean class selectivity index (compare to Figure A5d). (c) Test accuracy (y-axis) as a function of mean class selectivity (x-axis) for different values of α after removing dead units from the class selectivity calculation. Error bars denote 95% confidence intervals. $*p < 2 \times 10^{-4}$, $**p < 5 \times 10^{-7}$ difference from $\alpha = 0$ difference from $\alpha = 0$, t-test, Bonferroni-corrected. All results shown are for ResNet20.

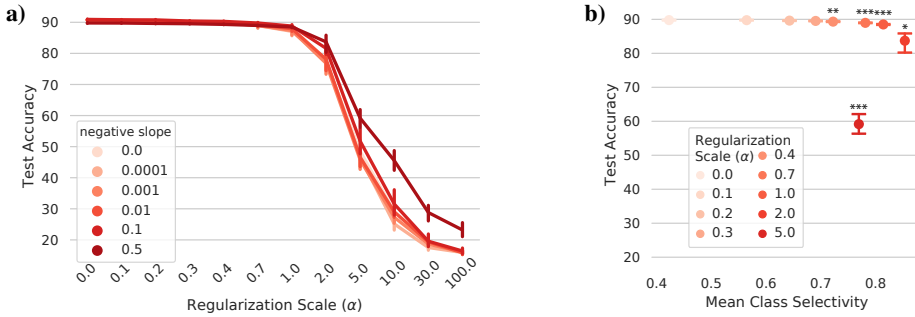


Figure A8: Reviving dead units does not rescue the performance deficits caused by increasing selectivity in ResNet20. (a) Test accuracy (y-axis) as a function of regularization scale (α ; x-axis) for different leaky-ReLU negative slopes (intensity of red). Leaky-ReLUs completely solve the dead unit problem but do not fully rescue test accuracy for networks with $\alpha > 0$. (b) Mean class selectivity index (y-axis) as a function of regularization scale (α ; x-axis and intensity of red) for leaky-ReLU negative slope = 0.5. $*p < 0.001$, $**p < 2 \times 10^{-4}$, $***p < 5 \times 10^{-10}$ difference from $\alpha = 0$, t-test, Bonferroni-corrected. Error bars denote bootstrapped 95% confidence intervals.

A.11 RULING OUT A DEGENERATE SOLUTION FOR INCREASING SELECTIVITY

One degenerate solution to generate a very high selectivity index is for a unit to be silent for the vast majority of inputs, and have low activations for the small set of remaining inputs. We refer to this scenario as "activation minimization". We verified that activation minimization does not fully account for our results by examining the proportion of activations which elicit non-zero activations in the units in our models. If our regularizer is indeed using activation minimization to generate high selectivity in individual units, then regularizing to increase class selectivity should cause most units to have non-zero activations for only a very small proportion of samples. In ResNet18 trained on Tiny ImageNet, we found that sparse units, defined as units that do not respond to at least half of the data samples, only constitute more than 10% of the total population at extreme positive regularization scales ($\alpha \geq 10$; Figures A9a, ??), well after large performance deficits $>4\%$ emerge (Figure 3). In ResNet20 trained on CIFAR10, networks regularized to have higher class selectivity (i.e. positive α) did indeed have more sparse units (Figures A9b, ??). However, this effect does not explain away our findings: by $\alpha = 0.7$, the majority of units respond to over 80% of samples (i.e. they are not sparse), but test accuracy has already decreased by 5% (Figure A6). These results indicate that activation minimization does not explain class selectivity-related changes in test accuracy.

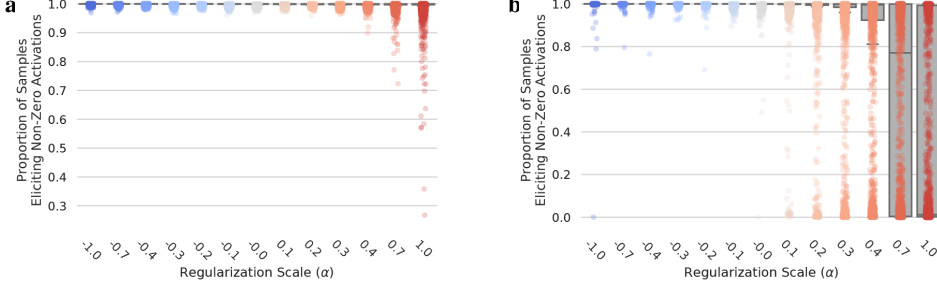


Figure A9: Activation minimization does not explain selectivity-induced performance changes. (a) Proportion of samples eliciting a non-zero activation (y-axis) vs. regularization scale (α ; x-axis) in ResNet18 trained on Tiny ImageNet. Data points denote individual units. Boxes denote IQR, whiskers extend $2 \times \text{IQR}$. Note that the boxes are very compressed because the distribution is confined almost entirely to $y=1.0$ for all values of x . (b) Identical to (a), but for ResNet20 trained on CIFAR10.

A.12 RESULTS FOR VGG16

Modulating class selectivity in VGG16 yielded results qualitatively similar to those we observed in ResNet20. The regularizer reliably decreases class selectivity for negative values of α (Figure A10), and class selectivity can be drastically reduced with little impact on test accuracy (Figure A11). Although test accuracy decreases significantly at $\alpha = -0.1$ ($p = 0.004$, Bonferroni-corrected t-test), the effect is small: it is possible to reduce mean class selectivity by a factor of 5 with only a 0.5% decrease in test accuracy, and by a factor of 10—to 0.03—with only a ~1% drop in test accuracy.

Regularizing to increase class selectivity also has similar effects in VGG16 and ResNet20. Increasing α causes class selectivity to increase, and the effect becomes less consistent at large values of α (Figure A5). Although the class selectivity-induced collapse in test accuracy does not emerge quite as rapidly in VGG16 as it does in ResNet20, the decrease in test accuracy is still significant at the smallest tested value of α ($\alpha = 0.1$, $p = 0.02$, Bonferroni-corrected t-test), and the effects on test accuracy of regularizing to promote vs. discourage class selectivity become significantly different at $\alpha = 0.3$ ($p = 10^{-4}$, Wilcoxon rank-sum test; Figure A14). Our observations that class selectivity is neither necessary nor sufficient for performance in both VGG16 and ResNet20 indicates that this is likely a general property of CNNs.

It is worth noting that VGG16 exhibits greater class selectivity than ResNet20. In the absence of regularization (i.e. $\alpha = 0$), mean class selectivity in ResNet20 is 0.22, while in VGG16 it is 0.35, a 1.6x increase. This could explain why positive values of α seem to have a stronger effect on class selectivity in VGG16 relative to ResNet20 (compare Figure A5 and Figure A12; also see Figure A26b).

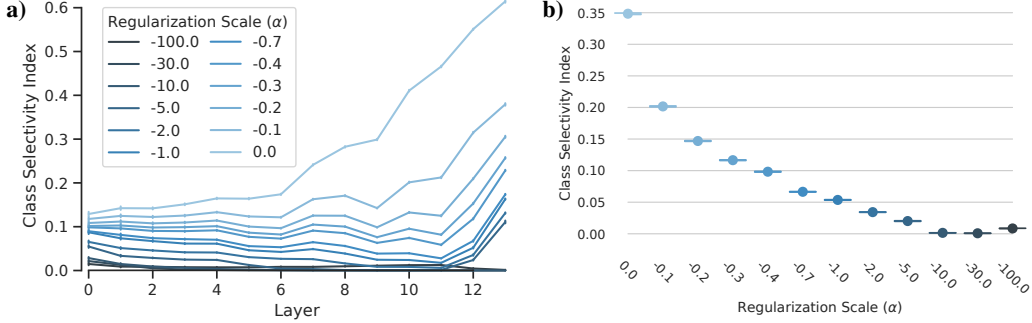


Figure A10: Regularizing to decrease class selectivity in VGG16. (a) Mean class selectivity index (y-axis) as a function of layer (x-axis) for different regularization scales (α ; denoted by intensity of blue) for VGG16. (b) Similar to (a), but mean is computed across all units in a network instead of per layer. Error bars denote bootstrapped 95% confidence intervals.

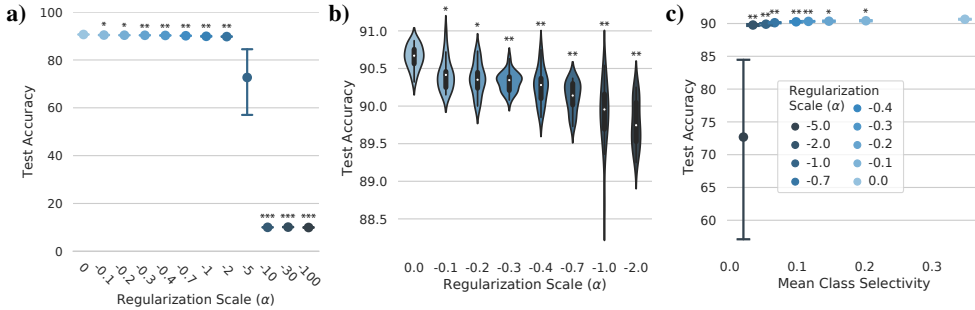


Figure A11: Effects of reducing class selectivity on test accuracy in VGG16. (a) Test accuracy (y-axis) as a function of regularization scale (α , x-axis and intensity of blue). (b) Identical to (a), but for a subset of α values. The center of each violin plot contains a boxplot, in which the darker central lines denote the central two quartiles. (c) Test accuracy (y-axis) as a function of mean class selectivity (x-axis) for different values of α . Error bars denote 95% confidence intervals. $*p < 0.005$, $**p < 5 \times 10^{-6}$, $***p < 5 \times 10^{-60}$ difference from $\alpha = 0$, t-test, Bonferroni-corrected. All results shown are for VGG16.

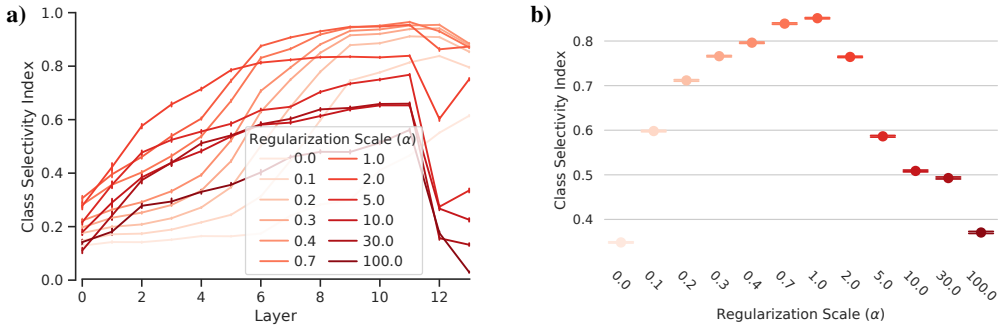


Figure A12: Regularizing to increase class selectivity in VGG16. (a) Mean class selectivity index (y-axis) as a function of layer (x-axis) for different regularization scales (α ; denoted by intensity of red) for VGG16. (b) Similar to (a), but mean is computed across all units in a network instead of per layer. Error bars denote bootstrapped 95% confidence intervals.

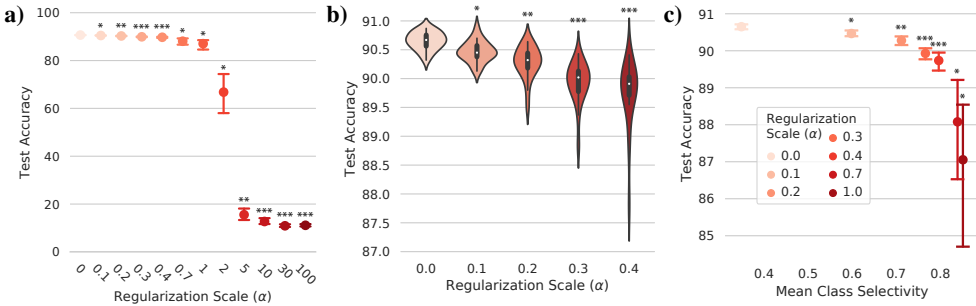


Figure A13: Effects of increasing class selectivity on test accuracy in VGG16. (a) Test accuracy (y-axis) as a function of regularization scale (α , x-axis and intensity of red). (b) Identical to (a), but for a subset of α values. The center of each violin plot contains a boxplot, in which the darker central lines denote the central two quartiles. (c) Test accuracy (y-axis) as a function of mean class selectivity (x-axis) for different values of α . Error bars denote 95% confidence intervals. $*p < 0.05$, $**p < 5 \times 10^{-4}$, $***p < 9 \times 10^{-6}$ difference from $\alpha = 0$, t-test, Bonferroni-corrected. All results shown are for VGG16.

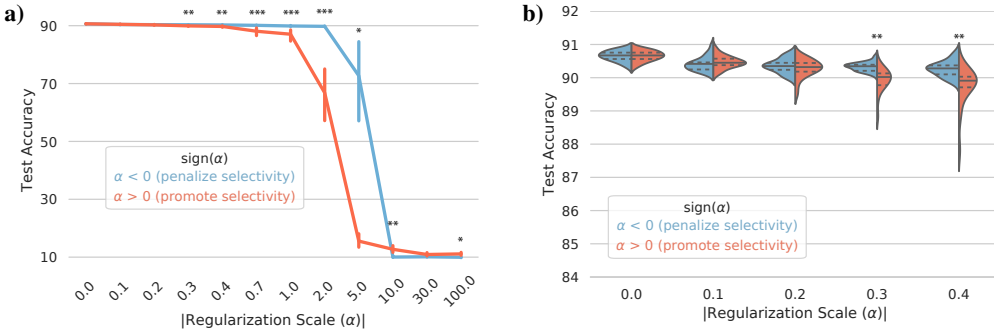


Figure A14: Regularizing to promote vs. penalize class selectivity in VGG16. (a) Test accuracy (y-axis) as a function of regularization scale magnitude ($|\alpha|$; x-axis) when promoting ($\alpha > 0$, red) or penalizing ($\alpha < 0$, blue) class selectivity in VGG16. Error bars denote bootstrapped 95% confidence intervals. (b) Identical to (a), but for a subset of $|\alpha|$ values. $*p < 0.05$, $**p < 10^{-3}$, $***p < 10^{-6}$ difference between $\alpha < 0$ and $\alpha > 0$, Wilcoxon rank-sum test, Bonferroni-corrected.

A.13 DIFFERENT SELECTIVITY METRICS

In order to confirm that the effect of the regularizer is not unique to our chosen class selectivity metric, we also examined the effect of our regularizer on the "precision" metric for class selectivity (Zhou et al., 2015; 2018; Gale et al., 2019). The precision metric is calculated by finding the N images that most strongly activate a given unit, then finding the image class C_i that constitutes the largest proportion of the N images. Precision is defined as this proportion. For example, if $N = 200$, and the "cats" class, with 74 samples, constitutes the largest proportion of those 200 activations for a unit, then the precision of the unit is $\frac{74}{200} = 0.34$. Note that for a given number of classes C , precision is bounded by $[\frac{1}{C}, 1]$, thus in our experiments the lower bound on precision is 0.1.

Zhou et al. (2015) used $N = 60$, while Gale et al. (2019) used $N = 100$. We chose to use the number of samples per class in the test set data and thus the largest possible sample size. This yielded $N = 1000$ for CIFAR10 and $N = 50$ for Tiny Imagenet.

The class selectivity regularizer has similar effects on precision as it does on the class selectivity index. Regularizing against class selectivity has a consistent effect on precision (Figure A15), while regularizing to promote class selectivity has a consistent effect in ResNet18 trained on Tiny ImageNet and for smaller values of α in ResNet20 trained on CIFAR10. However, the relationship between precision and the class selectivity index becomes less consistent for larger positive values of α in ResNet20 trained on CIFAR10. One explanation for this is that activation sparsity is a valid solution for maximizing the class selectivity index but not precision. For example, a unit that responded only to ten samples from the class "cat" and not at all to the remaining samples would have a class selectivity index of 1, but a precision value of 0.11. This seems likely given the increase in sparsity observed for very large positive values of α (see Appendix A.11).

While there are additional class selectivity metrics that we could have used to further assess the effect of our regularizer, many of them are based on relating the activity of a neuron to the accuracy of the network’s output(s) (e.g. top class selectivity Gale et al. (2019) and class correlation Li et al. (2015); Zhou et al. (2018)), confounding classification accuracy and class selectivity. Accordingly, these metrics are unfit for use in experiments that examine the relationship between class selectivity and classification accuracy, which is exactly what we do here.

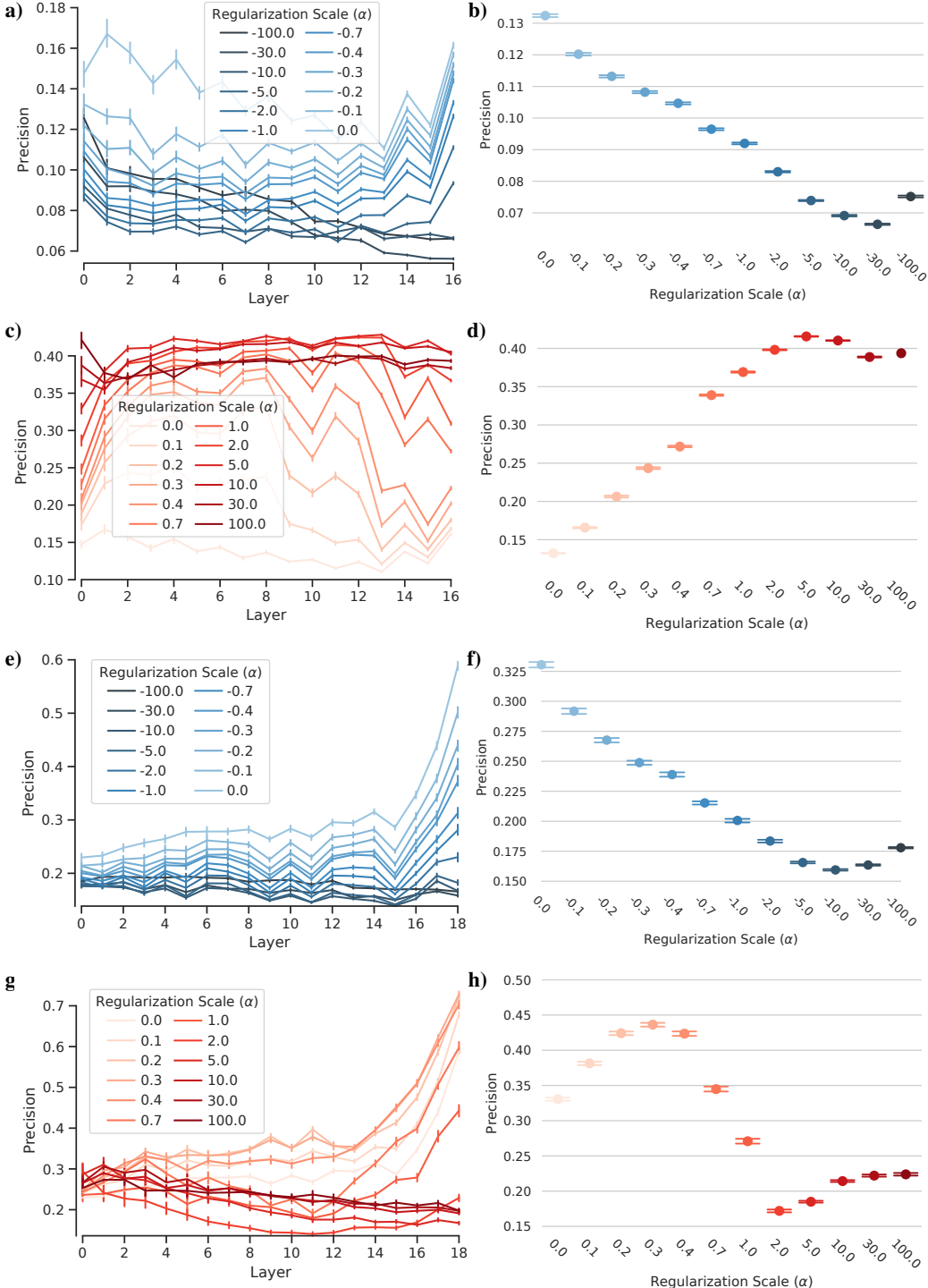


Figure A15: Class selectivity regularization has similar effects when measured using a different class selectivity metric. (a) Mean precision (y-axis) as a function of layer (x-axis) for different regularization scales (α ; denoted by intensity of blue) when regularizing against class selectivity in ResNet18. Precision is an alternative class selectivity metric (see Appendix A.13). (b) Similar to (a), but mean is computed across all units in a network instead of per layer. (c) and (d) are identical to (a) and (b), respectively, but when regularizing to promote class selectivity. (e-h) are identical to (a-d), respectively, but for ResNet20. Error bars denote bootstrapped 95% confidence intervals.

A.14 RESTRICTING CLASS SELECTIVITY REGULARIZATION TO THE FIRST THREE OR FINAL THREE LAYERS

To investigate the layer-specificity of the effects of class selectivity regularization, we also examined the effects of restricting class selectivity regularization to the first three or last three layers of the networks. Interestingly, we found that much of the effect of regularizing for or against selectivity on test accuracy was replicated even when the regularization was restricted to the first or final three layers. For example, reducing class selectivity in the first three layers either improves test accuracy—in ResNet18 trained on Tiny ImageNet—or has little-to-no effect on test accuracy—in ResNet20 trained on CIFAR10 (Figures A16 and A17). Likewise, regularizing to increase class selectivity in the first three layers had an immediate negative impact on test accuracy in both models (Figures A18 and A19). Regularizing against class selectivity in the final three layers (Figures A20 and A21) caused a modest increase in test accuracy over a narrow range of α in ResNet18 trained on Tiny ImageNet: less than half a percent gain at most (at $\alpha = -0.2$), and no longer present by $\alpha = -0.4$ (Figure A21b). In ResNet20, regularizing against class selectivity in the final three layers actually causes a decrease in test accuracy (Figures A17c and A17d). Given that the output layer of CNNs trained for image classification are by definition class-selective, we thought that regularizing to increase class selectivity in the final three layers could improve performance, but surprisingly it causes an immediate drop in test accuracy in both models (Figures A22 and A23). Our observation that regularizing to decrease class selectivity provides greater benefits (in the case of ResNet18) or less impairment (in the case of ResNet20) in the first three layers compared to the final three layers leads to the conclusion that class selectivity is less necessary (or more detrimental) in early layers compared to late layers.

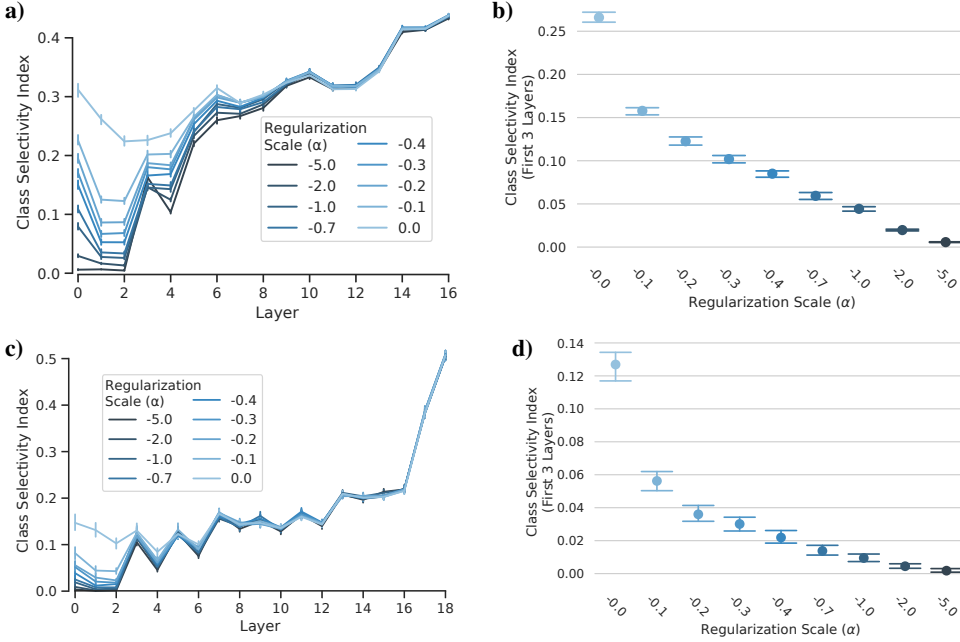


Figure A16: Regularizing to decrease class selectivity in the first three network layers. (a) Mean class selectivity (y-axis) as a function of layer (x-axis) for different values of α (intensity of blue) when class selectivity regularization is restricted to the first three network layers in ResNet18 trained on Tiny ImageNet. (b) Mean class selectivity in the first three layers (y-axis) as a function of α (x-axis) in ResNet18 trained on Tiny ImageNet. (c) and (d) are identical to (a) and (b), respectively, but for ResNet20 trained on CIFAR10. Error bars = 95% confidence intervals.

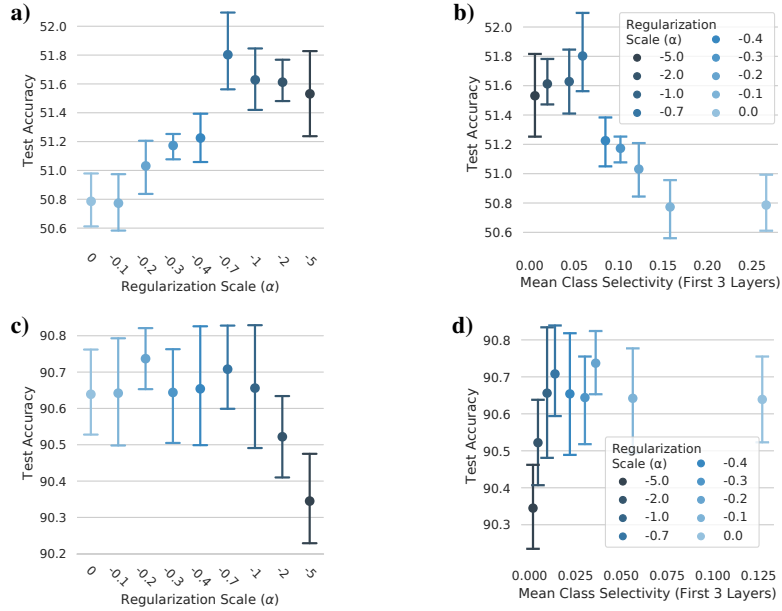


Figure A17: Effects on test accuracy when regularizing to decrease class selectivity in the first three network layers. (a) Test accuracy (y-axis) as a function of α (x-axis) when class selectivity regularization is restricted to the first three network layers in ResNet18 trained on Tiny ImageNet. (b) Test accuracy (y-axis) as a function of mean class selectivity in the first three layers (x-axis) in ResNet18 trained on Tiny ImageNet. (c) and (d) are identical to (a) and (b), respectively, but for ResNet20 trained on CIFAR10. Error bars = 95% confidence intervals.

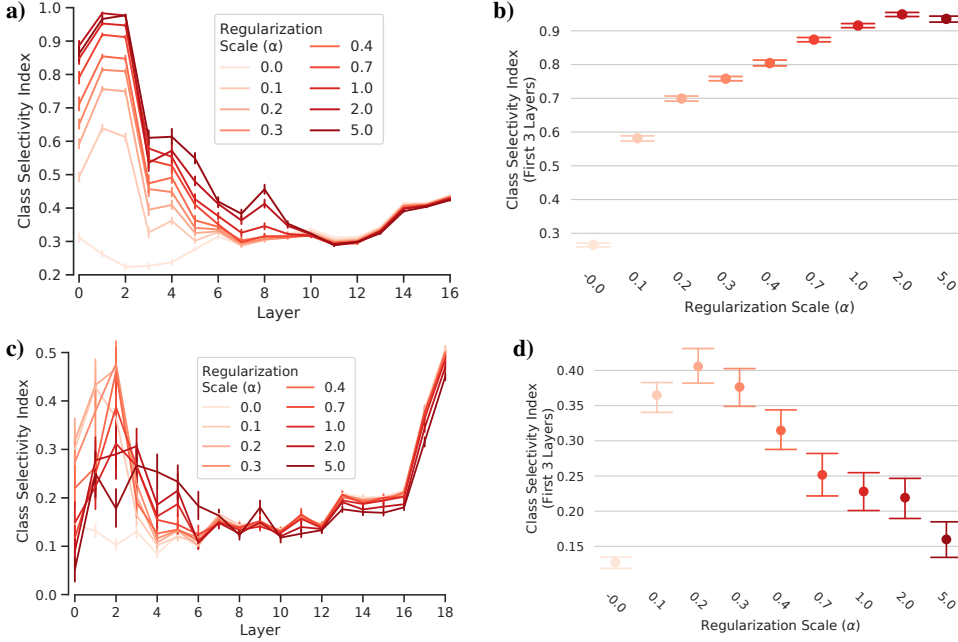


Figure A18: Regularizing to increase class selectivity in the first three network layers. (a) Mean class selectivity (y-axis) as a function of layer (x-axis) for different values of α (intensity of red) when class selectivity regularization is restricted to the first three network layers in ResNet18 trained on Tiny ImageNet. (b) Mean class selectivity in the first three layers (y-axis) as a function of α (x-axis) in ResNet18 trained on Tiny ImageNet. (c) and (d) are identical to (a) and (b), respectively, but for ResNet20 trained on CIFAR10. Error bars = 95% confidence intervals.

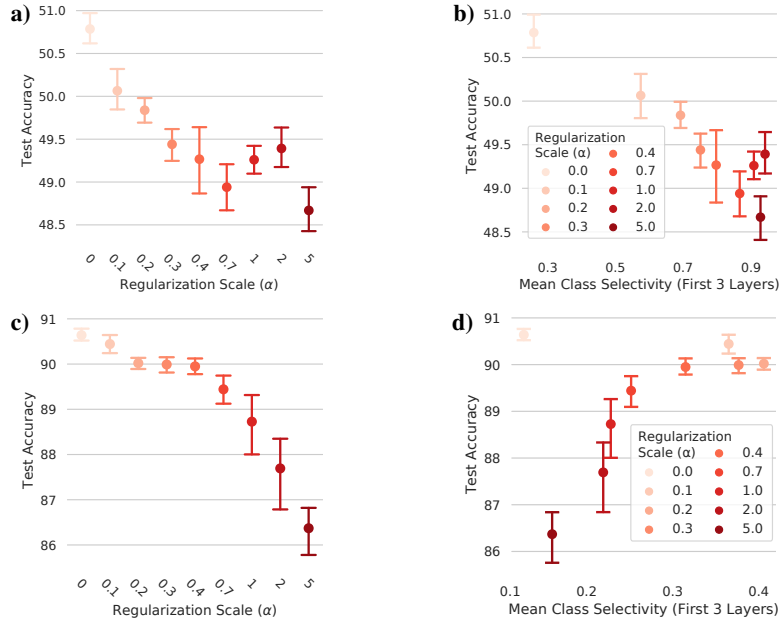


Figure A19: Effects on test accuracy when regularizing to increase class selectivity in the first three network layers. (a) Test accuracy (y-axis) as a function of α (x-axis) when class selectivity regularization is restricted to the first three network layers in ResNet18 trained on Tiny ImageNet. (b) Test accuracy (y-axis) as a function of mean class selectivity in the first three layers (x-axis) in ResNet18 trained on Tiny ImageNet. (c) and (d) are identical to (a) and (b), respectively, but for ResNet20 trained on CIFAR10. Error bars = 95% confidence intervals.

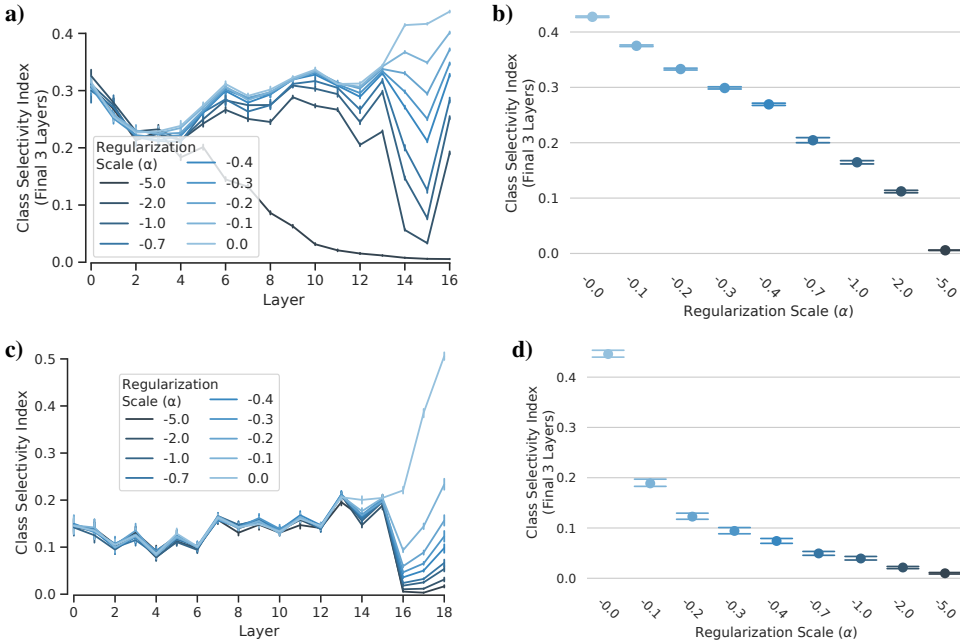


Figure A20: Regularizing to decrease class selectivity in the last three network layers. (a) Mean class selectivity (y-axis) as a function of layer (x-axis) for different values of α (intensity of blue) when class selectivity regularization is restricted to the last three network layers in ResNet18 trained on Tiny ImageNet. (b) Mean class selectivity in the last three layers (y-axis) as a function of α (x-axis) in ResNet18 trained on Tiny ImageNet. (c) and (d) are identical to (a) and (b), respectively, but for ResNet20 trained on CIFAR10. Error bars = 95% confidence intervals.

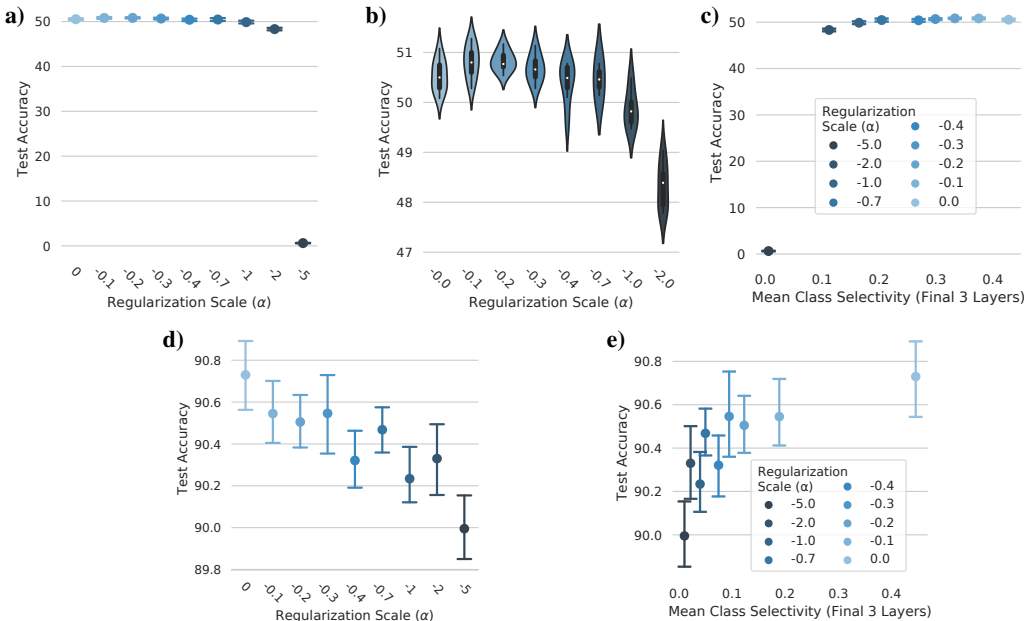


Figure A21: Effects on test accuracy when regularizing to decrease class selectivity in the last three network layers. (a) Test accuracy (y-axis) as a function of α (x-axis) when class selectivity regularization is restricted to the last three network layers in ResNet18 trained on Tiny ImageNet. (b) Similar to (a), but for a subset of α values. (c) Test accuracy (y-axis) as a function of mean class selectivity in the last three layers (x-axis) in ResNet18 trained on Tiny ImageNet. (d) and (e) are identical to (a) and (c), respectively, but for ResNet20 trained on CIFAR10. Error bars = 95% confidence intervals.

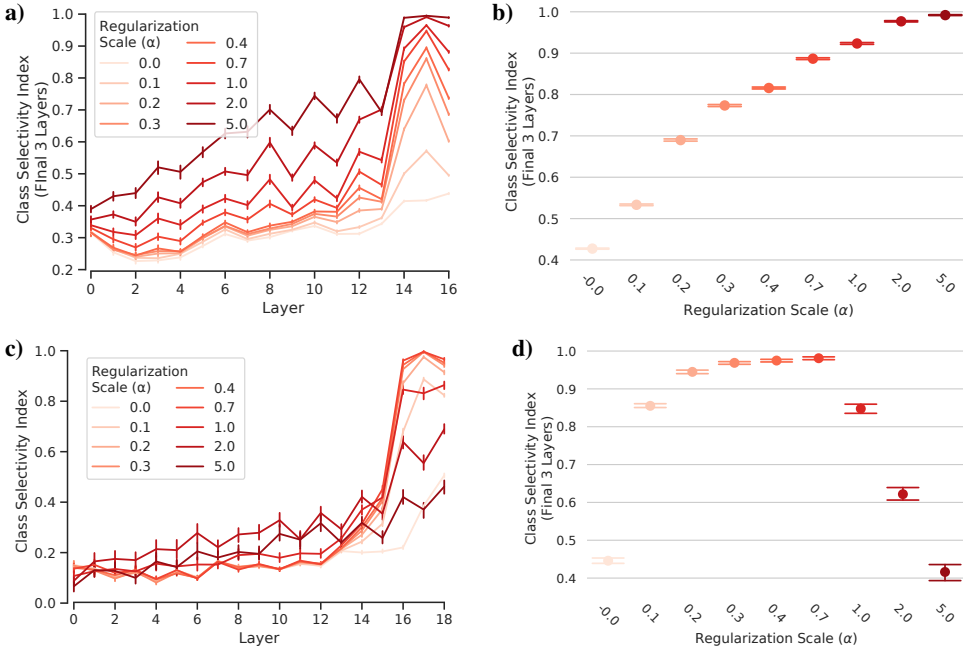


Figure A22: Regularizing to increase class selectivity in the last three network layers. (a) Mean class selectivity (y-axis) as a function of layer (x-axis) for different values of α (intensity of red) when class selectivity regularization is restricted to the last three network layers in ResNet18 trained on Tiny ImageNet. (b) Mean class selectivity in the last three layers (y-axis) as a function of α (x-axis) in ResNet18 trained on Tiny ImageNet. (c) and (d) are identical to (a) and (b), respectively, but for ResNet20 trained on CIFAR10. Error bars = 95% confidence intervals.

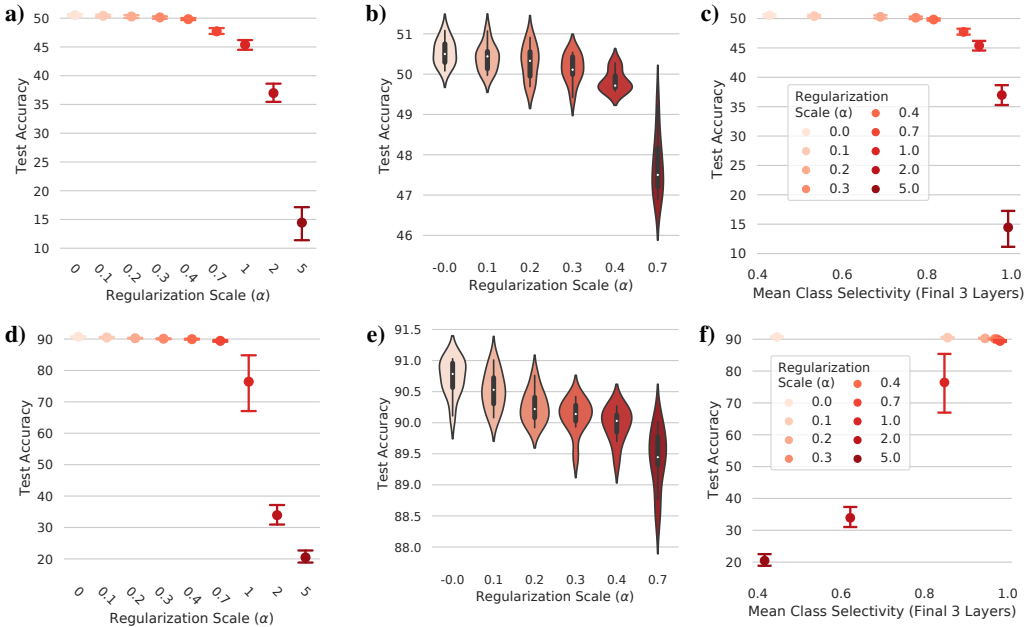


Figure A23: Effects on test accuracy when regularizing to increase class selectivity in the last three network layers. (a) Test accuracy (y-axis) as a function of α (x-axis) when class selectivity regularization is restricted to the last three network layers in ResNet18 trained on Tiny ImageNet. (b) Similar to (a), but for a subset of α values. (c) Test accuracy (y-axis) as a function of mean class selectivity in the last three layers (x-axis) in ResNet18 trained on Tiny ImageNet. (d-f) are identical to (a-c), respectively, but for ResNet20 trained on CIFAR10. Error bars = 95% confidence intervals.

A.15 ADDITIONAL RESULTS

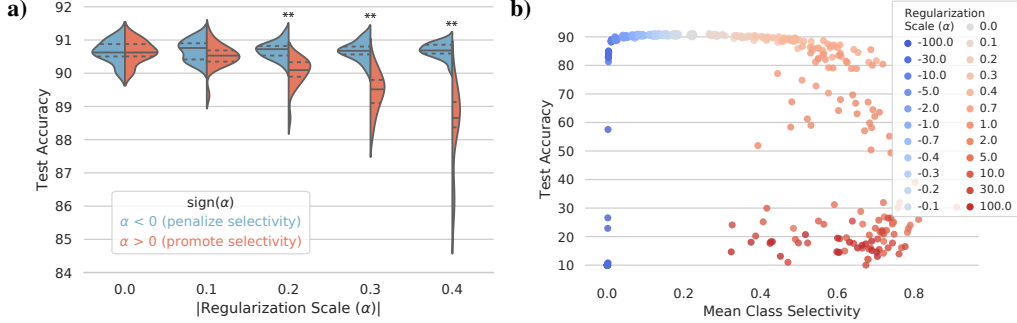


Figure A24: Increasing class selectivity has rapid and deleterious effects on test accuracy compared to reducing class selectivity in ResNet20 trained on CIFAR10. (a) Test accuracy (y-axis) as a function of regularization scale magnitude ($|\alpha|$) for negative (blue) vs positive (red) values of α . Solid line in distributions denotes mean, dashed line denotes central two quartiles. ** $p < 6 \times 10^{-6}$ difference between $\alpha < 0$ and $\alpha > 0$, Wilcoxon rank-sum test, Bonferroni-corrected. (b) Test accuracy (y-axis) as a function of mean class selectivity (x-axis).

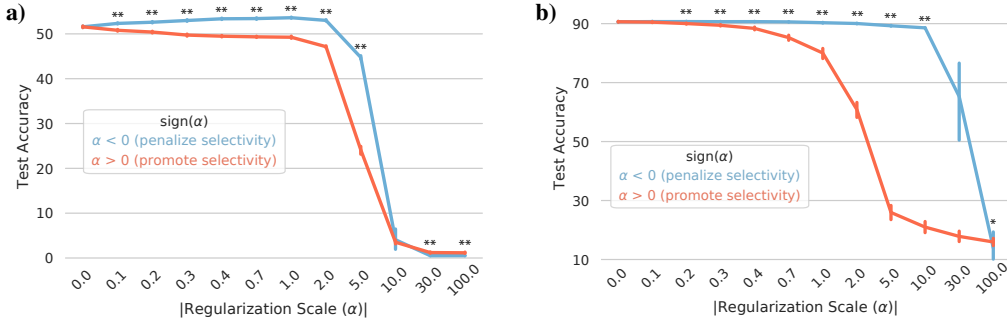


Figure A25: Directly comparing promoting vs penalizing class selectivity. (a) Test accuracy (y-axis) as a function of regularization scale (α ; x-axis) when promoting ($\alpha > 0$, red) or penalizing ($\alpha < 0$, blue) class selectivity in ResNet18 trained on Tiny Imagenet. ** $p < 2 \times 10^{-5}$ difference between penalizing vs. promoting selectivity, Wilcoxon rank-sum test, Bonferroni-corrected. (b) same as (a) but for ResNet20 trained on CIFAR10. * $p < 0.05$, ** $p < 6 \times 10^{-6}$ difference, Wilcoxon rank-sum test, Bonferroni-corrected. Error bars denote bootstrapped 95% confidence intervals.

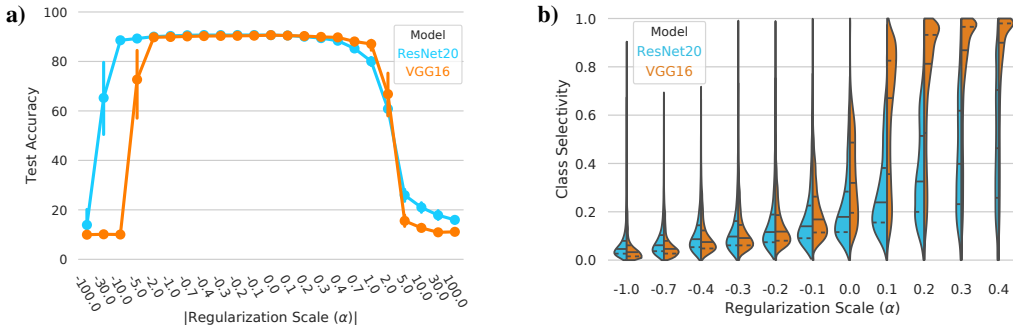


Figure A26: Differences between ResNet20 and VGG16. (a) Test accuracy (y-axis) as a function of regularization scale (α x-axis) for ResNet20 (cyan) and VGG16 (orange). Error bars denote bootstrapped 95% confidence intervals. (b) Class selectivity (y-axis) as a function of regularization scale (α for Resnet20 (cyan) and VGG16 (orange)).